The Journal of Experimental Biology 200, 1549–1569 (1997)
Printed in Great Britain © The Company of Biologists Limited 1997
JEB0850

LABRIFORM PROPULSION IN FISHES: KINEMATICS OF FLAPPING AQUATIC FLIGHT IN THE BIRD WRASSE *GOMPHOSUS VARIUS* (LABRIDAE)

JEFFREY A. WALKER* AND MARK W. WESTNEAT

Department of Zoology and Center for Environmental and Evolutionary Biology, Field Museum of Natural History, Roosevelt Road at Lake Shore Drive, Chicago, IL 60605, USA

Accepted 14 March 1997

Summary

Labriform, or pectoral fin, propulsion is the primary swimming mode for many fishes, even at high relative speeds. Although kinematic data are critical for evaluating hydrodynamic models of propulsion, these data are largely lacking for labriform swimmers, especially for species that employ an exclusively labriform mode across a broad range of speeds. We present data on pectoral fin locomotion in *Gomphosus varius* (Labridae), a tropical coral reef fish that uses a lift-based mechanism to fly under water at sustained speeds of 1–6 total body lengths s^{-1} (*TL* s^{-1}). Lateral- and dorsal-view video images of three fish swimming in a flow tank at 1–4 *TL* s^{-1} were recorded at 60 Hz. From the two views, we reconstructed the three-dimensional motion of the center of mass, the fin tip and two fin chords for multiple fin beats of each fish at each of four speeds. In *G. varius*, the fin oscillates largely up and down: the stroke plane is tilted by approximately 20 ° from the vertical. Both frequency and the area swept by the pectoral fins increase with swimming speed. Interestingly, there are individual differences in how this area increases. Relative to the fish, the fin tip in lateral view moves along the path of a thin, inclined figure-of-eight. Relative to a stationary observer, the fin tip traces a sawtooth pattern, but the teeth are recumbent (indicating net backwards movement) only at the slowest speeds. Distal fin chords pitch nose downward during the downstroke and nose upward during the upstroke. Hydrodynamic angles of attack are largely positive during the downstroke and negative during the upstroke. The geometry of the fin and incident flow suggests that the fin is generating lift with large upward and small forward components during the downstroke. The negative incident angles during the upstroke suggest that the fin is generating largely thrust during the upstroke. In general, the large thrust is combined with a downward force during the upstroke, but the net backwards motion of the fin at slow speeds generates a small upward component during slow swimming. Both the alternating sign of the hydrodynamic angle of attack and the observed reduced frequencies suggest that unsteady effects are important in *G. varius* aquatic flight, especially at low speeds. This study provides a framework for the comparison of aquatic flight by fishes with aerial flight by birds, bats and insects.

Key words: fish, locomotion, pectoral fin propulsion, swimming, hydrodynamics, kinematics, speed effects, bird wrasse, *Gomphosus varius*.

Introduction

The kinematics and dynamics of locomotion using paired oscillating appendages have been intensively investigated in flying animals, including birds, bats and insects, but have received comparatively little attention in their swimming relatives (see Vogel, 1994). Most research programs in fish locomotion have focused on axial mechanisms (see Videler, 1993). Many fishes, however, use oscillating pectoral fins for maneuvering and rectilinear motion at low swimming speeds (Lindsey, 1978). Several large families of marine fishes from the order Perciformes have members that employ flapping pectoral fins, to the exclusion of median and caudal fins, for relatively high-speed swimming. These families include the Acanthuridae (surgeonfishes), Embiotocidae (surfperches), Scaridae (parrotfishes) and Labridae (wrasses).

Animals flying through air generate thrust as a consequence of the aerodynamic lift produced on the surface of the flapping wings. Importantly, the net resultant force also has an upward component that keeps the animal aloft. Most fishes are nearly neutrally buoyant and have less need, compared with flying animals, to couple large upward forces with thrust production. As a consequence, fishes have evolved a diverse array of propulsive structures (Breder, 1926; Lindsey 1978), each of which can generate thrust by multiple hydrodynamic mechanisms (Lighthill, 1975; Blake, 1983*a*,*b*; Webb, 1982, 1984, 1988; Webb and Blake, 1985; Daniel *et al.* 1992).

Harris (1937) outlined qualitatively some basic mechanisms of force production from paired oscillating or undulating pectoral fins. Recent studies of pectoral fin propulsion have

*e-mail: walker@fmppr.fmnh.org.

focused on stroke parameters (Webb, 1973; Archer and Johnston, 1989; Drucker and Jensen, 1996) or have not provided the necessary suite of kinematic variables with which to draw rigorous hydrodynamic conclusions (Geerlink, 1983; Gibb *et al.* 1994). The one notable exception is the work of Blake (1979*a*, 1980), who described the kinematics of the oscillating fin in the angelfish *Pterophyllum eimekei* in sufficient detail to model a drag-based mechanism of thrust generation. In a drag-based stroke, pectoral fin movement resembles the rowing motion of an oar (Breder, 1926): during abduction, the fin is brought forward with its surface parallel to fin movement, and during adduction, the fin is pulled back with its surface normal to its movement. Resistance to backward rotation of the fin during adduction is felt as thrust at the center of mass. The rotating fin also accelerates a mass of water, causing a reaction force in the opposite direction. For example, the fin at the start of adduction accelerates a mass of water backwards, creating a reaction force propelling the fish forwards. Although rowing is referred to as 'drag-based', at the Reynolds numbers (*Re*) encountered by most swimming fish, the acceleration reaction force is likely to dominate the drag force in magnitude (Daniel, 1984; Daniel and Meyhöfer, 1989).

Webb (1973) recognized that the fin stroke of the shiner surfperch *Cymatogaster aggregata* resembled the wingbeat of flying birds, suggesting that the surfperch generates thrust *via* a lift-based mechanism. This lift-based fin stroke is characterized by the largely up-and-down flapping of the fin (Breder, 1926) with small changes in fin pitch to maintain optimal attack angles. Blake (1983*a*,*b*) applied a simple lift-based model to the *C. aggregata* fin stroke, but a full kinematic and hydrodynamic analysis was never published. In the present paper, we describe the detailed motions of the flapping pectoral fin across a range of speeds in the bird wrasse *Gomphosus varius*. The bird wrasse is a member of the 'type' family of labriform swimmers, the Labridae. Labrids present an unusual diversity of fin shapes and pectoral fin kinematics and are, therefore, a good model system with which to investigate the evolution of pectoral fin propulsion. In this study, we explored the effects of swimming speed on stroke parameters and investigated the instantaneous movement of the pectoral fin in sufficient detail to allow the construction of a preliminary hydrodynamic hypothesis of lift-based pectoral fin propulsion in fishes.

Materials and methods

The bird wrasse *Gomphosus varius* Lacépède is an active diurnal carnivore inhabiting tropical Indo-Pacific coral reefs. Its common name apparently refers to the elongated snout, which is used to probe for small benthic prey. The body is elongated and laterally compressed. The pectoral fins are broadest near the base, taper distally and have an aspect ratio of approximately 4.1 (measured as the square of the length of the fin divided by fin area). The base of the fin articulates with the shoulder at an angle of approximately 45° above the horizontal. Bird wrasses are negatively buoyant: the mean weight of anesthetized fish in water is 2.4±0.4 % (mean ± S.D., N=3) of the weight measured in air.

Individual fish were purchased through tropical marine fish wholesalers in Chicago, transported to the laboratory, and maintained in 200 l aquaria at 25 °C. We used a Panasonic AG-450 S-VHS camcorder to film the movements of individual fish swimming in a flow tank (Vogel and LaBarbera, 1978) at four flow speeds (22, 35, 47 and 59 cm s^{-1}). Two 250 W lights were used to illuminate the swimming arena. The working dimensions of the flow tank were 30 cm×30 cm×120 cm (108 l). A mirror mounted in the tank at 45° allowed simultaneous viewing of the lateral and dorsal surfaces of the fish. A centimeter grid was placed on the bottom and back of the tank to calibrate the video images. Water temperature in the flow tank was maintained at 25±1 °C.

Fin beats were digitized using an Apple Macintosh computer. A TelevEyes/Pro video scan converter with genlock (Digital Vision Corp.) was used to superimpose the computer monitor display and the video images onto an external Sony PVM-1340 monitor. Video sequences were played back at 60 video fields s^{-1} using a Panasonic AG-1970 SVHS player.

Prior to filming, fish were anesthetized in Finquel (Aldrich Chemical Co.), and tiny aluminum clips were attached to the fins to mark the desired landmarks for the digitizing procedure. The fish were allowed to recover fully before filming. We marked five fin landmarks (Fig. 1) and an estimate of the position of the center of mass. The fin markers are referred to as the leading-edge proximal marker, leading-edge distal marker, fin-tip marker, trailing-edge distal marker and trailing-edge proximal marker. The pairs of markers define the proximal and distal anatomical chords of the pectoral fin (Fig. 1). The center of mass was estimated using a tilt balance. The five fin markers and the dorsal base of the pectoral fin were digitized from both lateral and dorsal views. Three-dimensional Cartesian coordinates of the fin landmarks were constructed from their positions in the pairs of two-dimensional views.

The fin clips caused a distinct asymmetry of pectoral fin kinematics between marked and unmarked fins in some individuals. We analyzed only individuals that presented no apparent asymmetry throughout the entire experiment. Digitized sequences were obtained at all test speeds for three individuals (Table 1). We digitized fin beats in which the individual was swimming at least 5 cm above the bottom of the tank. Care was taken to digitize sequences in which the individual presented minimal (<5°) pitch, yaw and roll.

Summaries of stroke parameters may be confounded by differences in the total length (*TL*) of the individuals. We do not have enough data to characterize and adjust for allometry properly; hence, stroke parameters were computed for the three fish separately. All statistics on stroke parameters were performed in JMP 3.1 for the Macintosh (SAS Inc.).

We have not attempted a detailed hydrodynamic analysis of individual sequences. To identify the major kinematic trends, we present a summary of all collected data instead of 'representative' sequences. We used box plots to summarize changes in instantaneous kinematic parameters across all sequences, speeds and individuals. In these plots, time, on the abscissa, has been standardized so that the length of abduction

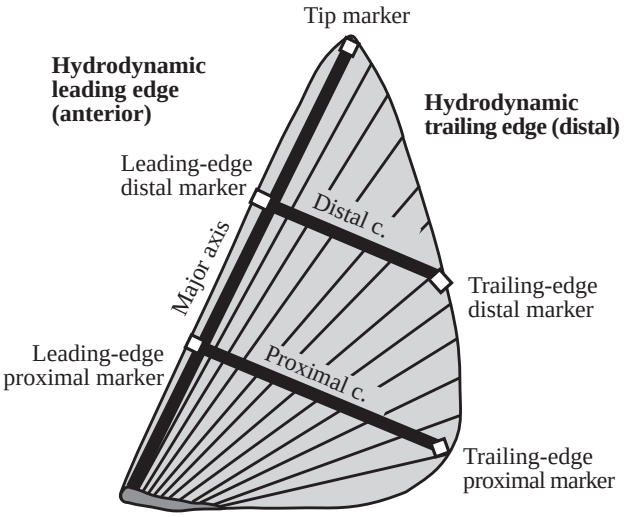

Fig. 1. Approximate locations of the five fin markers. The distal chord (Distal c.) is located at two-thirds of the length of the fin. The proximal chord (Proximal c.) is located at the widest portion of the fin.

and adduction are both unity. The standardized fields were binned into ten equally spaced time divisions for the abduction phase and six equally spaced time divisions for the adduction phase. Data from all fish and all trials within each speed were pooled. Standard quartiles were computed for each of the 15 time divisions for each of the four flow-tank velocities.

Results

General observations

When swimming, *Gomphosus varius* is extremely active. Unlike many other fishes, *G. varius* does not hover in the water column and we were unable to stimulate individuals to swim at constant velocities below approximately $1.2\,TL\,s^{-1}$. At velocities below this, *G. varius* accelerates, glides, turns laterally or pitches up or down using a combination of both pectoral fin and axial movements. *G. varius* moved using flapping of the pectoral fins exclusively at all test velocities. The highest velocities we measured were near $4\,TL\,s^{-1}$. Ongoing work in our laboratory suggests (1) that bird wrasses employ a strictly labriform mode of locomotion until fatigue velocity is reached and (2) that $4\,TL\,s^{-1}$ is well below the maximum sustainable swimming speeds ($6–7\,TL\,s^{-1}$) for the size range of individuals investigated here.

G. varius flapped its pectoral fins up and down with a small anterior movement during abduction and posterior movement during adduction (Figs 2, 3). Because the dorsoventral displacement of the fin tip far exceeded the fore–aft displacement, we often refer to abduction and adduction as the downstroke and upstroke, respectively. Note that isolated views of the flapping fin are similar to the fin geometry expected during a rowing stroke (Fig. 2). The fins flapped synchronously during rectilinear motion at all test speeds. Flapping frequency increased linearly with speed in all three individuals (Fig. 4; Table 2). The mean frequency was 2.9 Hz at $22\,cm\,s^{-1}$ and 4.2 Hz at $59\,cm\,s^{-1}$. The adduction phase accounted for between 23 and 46 % of the stroke cycle, but there was no association between this variable and swimming speed in any fish (Table 2).

Table 1. *Morphometric variables measured for each fish and mean hydrodynamic variables for each of* N *digitized sequences*

Individual	*N*	*TL* (cm)	Mass (g)	*U* ($cm\,s^{-1}$)	*Re*	*k*
1	9	18.0	50.6	22	3668	0.56
				35	5608	0.40
				47	7568	0.35
				59	10588	0.28
2	11	13.8	24.6	22	2628	0.48
				35	4122	0.39
				47	5394	0.33
				59	6576	0.28
3	10	15.9	43.9	22	3123	0.63
				35	5038	0.40
				47	6554	0.35
				59	8171	0.31

TL is total length; *U* is flow tank speed; *Re* is the Reynolds number estimated for the mean chord; *k* is the reduced frequency parameter for the mean chord (Spedding, 1992), where $k=\omega\bar{c}/(2U_{fish})$, ω is the angular frequency, $2\pi n$, where *n* is the stroke frequency, U_{fish} is the speed of the fish and $\bar{c}$ is mean chord. Mean chord was measured as fin area divided by fin length.

The distance travelled during a single fin stroke is the stride length, λ_s, which increased with velocity in all three fish (results not shown). Mean stride length was $0.46TL$ at $22\,cm\,s^{-1}$ and $0.89TL$ at $59\,cm\,s^{-1}$.

Stroke plane parameters

The configurations of the digitized fin markers were translated to superimpose the fin base landmark at the origin. Following this translation, the three-dimensional scatter of points for the tip marker reflects the oscillatory movement of the marker along the surface of a sphere with a radius equal to the distance from the marker to the fin base.

The motion of the tip marker is largely confined to oscillation along a single arc on the sphere. An arc on a sphere is a segment of the intersection between the sphere and a plane through the sphere. For the fin-tip marker, this plane is the stroke plane.

The stroke plane, as traditionally defined in insects (Jensen, 1956), (1) includes the base of the wing, (2) intersects a frontal plane orthogonal to the anterior–posterior axis of the body, and (3) intersects a sagittal plane by the inclination of the wing-tip trace in lateral projection relative to the body. We used the major axis of the scatter of the fin-tip points in lateral projection relative to the body to estimate the inclination of the stroke plane or stroke plane angle, β, from a positive dorsal unit vector.

$$\beta = \frac{\pi}{2} - \tan^{-1}\left[\frac{s_{zz} - s_{xx} + \sqrt{(s_{zz} - s_{xx})^2 + (2s_{xz})^2}}{2s_{xz}}\right], \quad (1)$$

where *s* is the (co)variance of the errors and β is numerically equivalent to the angle between the flapping and *x* axes

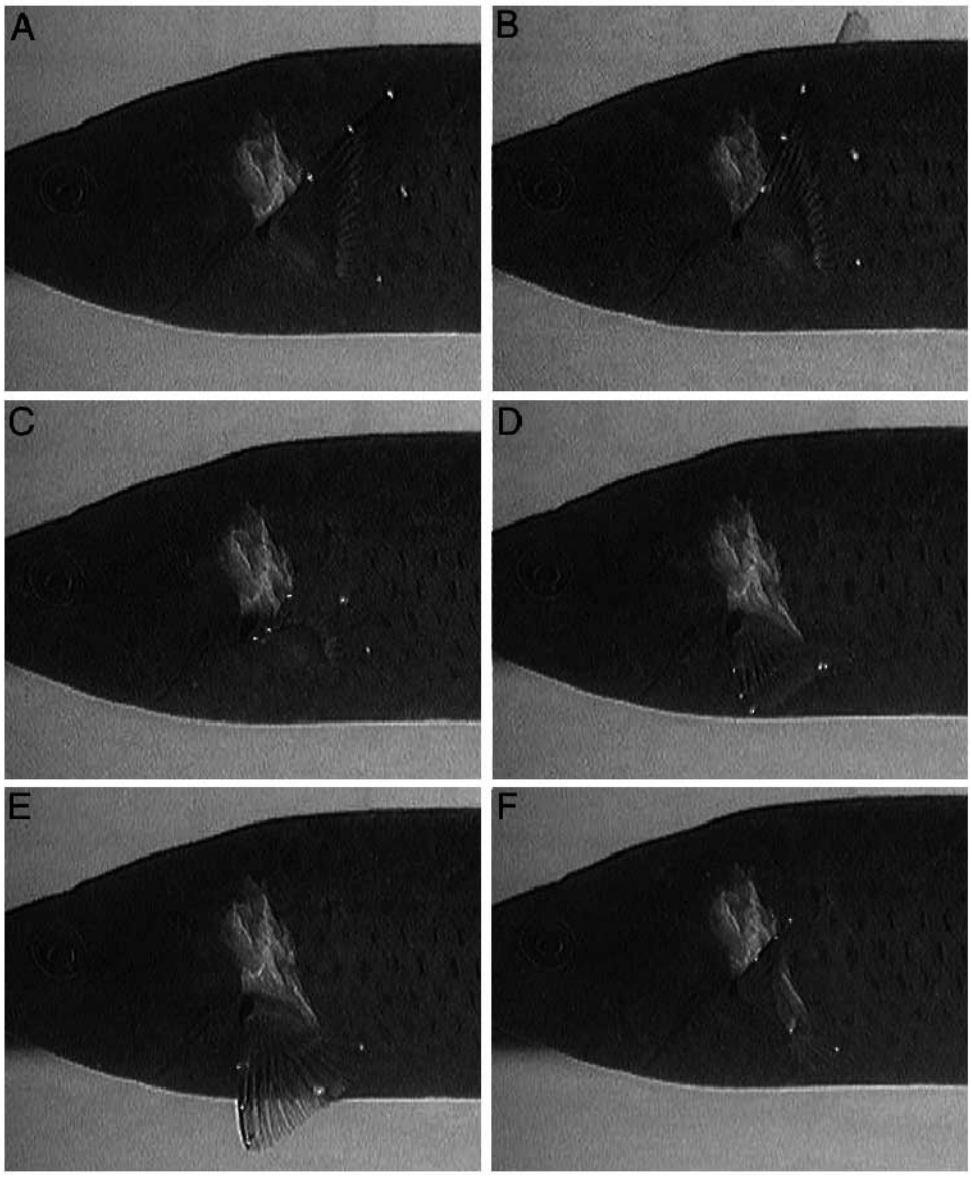

Fig. 2. Video image of a single fin beat of *Gomphosus varius* while swimming at 22 cm s^{-1}. (A) Maximum adduction. (B) Early phase II (the downstroke). Note that the fin has protracted forward. (C) Mid-phase II. Note the dorsal convexity of the fin. (D) Late phase II. Note the nose-down pitching of the distal fin. (E) Phase III. Note the protraction of the fin. (F) Mid-phase IV. Note the anteroventral convexity of the fin. Finally, note that isolated images of the fin can give a misleading interpretation of the mode of labriform propulsion (rowing *versus* flapping). For example, the fin in C or D appears to be feathered (which is distinct to rowing), while the fin in F appears to be rotating rapidly backwards with the blade normal to the flow (again, distinct to rowing). In reality, the fin in C and D has moderate hydrodynamic angles of attack (see Fig. 14), and the fin in F is moving dorsally rapidly at a small angle to its motion.

(Fig. 3A). The mean value of β was 19.4°. β decreased significantly by approximately 10° from the lowest to the highest speed in individual 1 but had no association with speed in the other two individuals (Table 2).

The major axis of the fin of *G. varius* (the leading-edge ray) does not oscillate back and forth on the stroke plane but sweeps back and forth along the edge of a cone whose vertex is the dorsal base of the fin (Fig. 3D). A similar geometry is also observed in the hindwing of the dragonfly (Azuma and Watanabe, 1988). In *G. varius*, the fin-tip marker oscillates, with some deviation, along an arc of the cone's base (Fig. 3D). We, therefore, defined the stroke plane as the plane containing the base of the stroke cone. In this geometry, the flapping axis, about which the fin rotates, is the central axis of the cone.

In order to estimate the orientation of the stroke plane, we used principal components analysis (PCA). Eigenvectors were computed from the covariance matrix of the scatter of the fin-tip marker coordinates translated to center the fin base at the origin. Using this method, we confirmed that the path of the fin tip is largely confined to a single plane: the percentage of total variance explained by the third principal component, a measure of the deviation of the fin tip from the stroke plane, was very small for all digitized sequences (mean percentage of variation explained by the first two principal components was 99±0.13 %; mean ± S.D.).

The first two eigenvectors, with elements e_i, were used to compute an equation for the stroke plane of the form:

$$xe_1 + ye_2 + ze_3 + d = 0, \quad (2)$$

where x, y and z are the components of a vector normal to the stroke plane and d is a constant. The angle β_{xz}, between the intersection of the stroke plane with the x,z plane and a positive dorsal unit vector is:

$$\beta_{xz} = \tan^{-1}(-x/z). \quad (3)$$

The angle, β_{xy}, between the intersection of the stroke and *x*,*y* planes and a positive lateral unit vector is:

$$\beta_{xy} = \tan^{-1}(y/x) . \quad (4)$$

The sign of these angles is indicated in Fig. 3B,C. In individual 2, both angles increase significantly with speed, but no significant associations are observed in the other individuals (Table 2).

If the assumptions of the traditionally defined stroke plane were true, β and β_{xz} would be equivalent. In fact, the values of β_{xz} are lower than β and are negative for some of the sequences. A negative β_{xz} indicates that the stroke plane

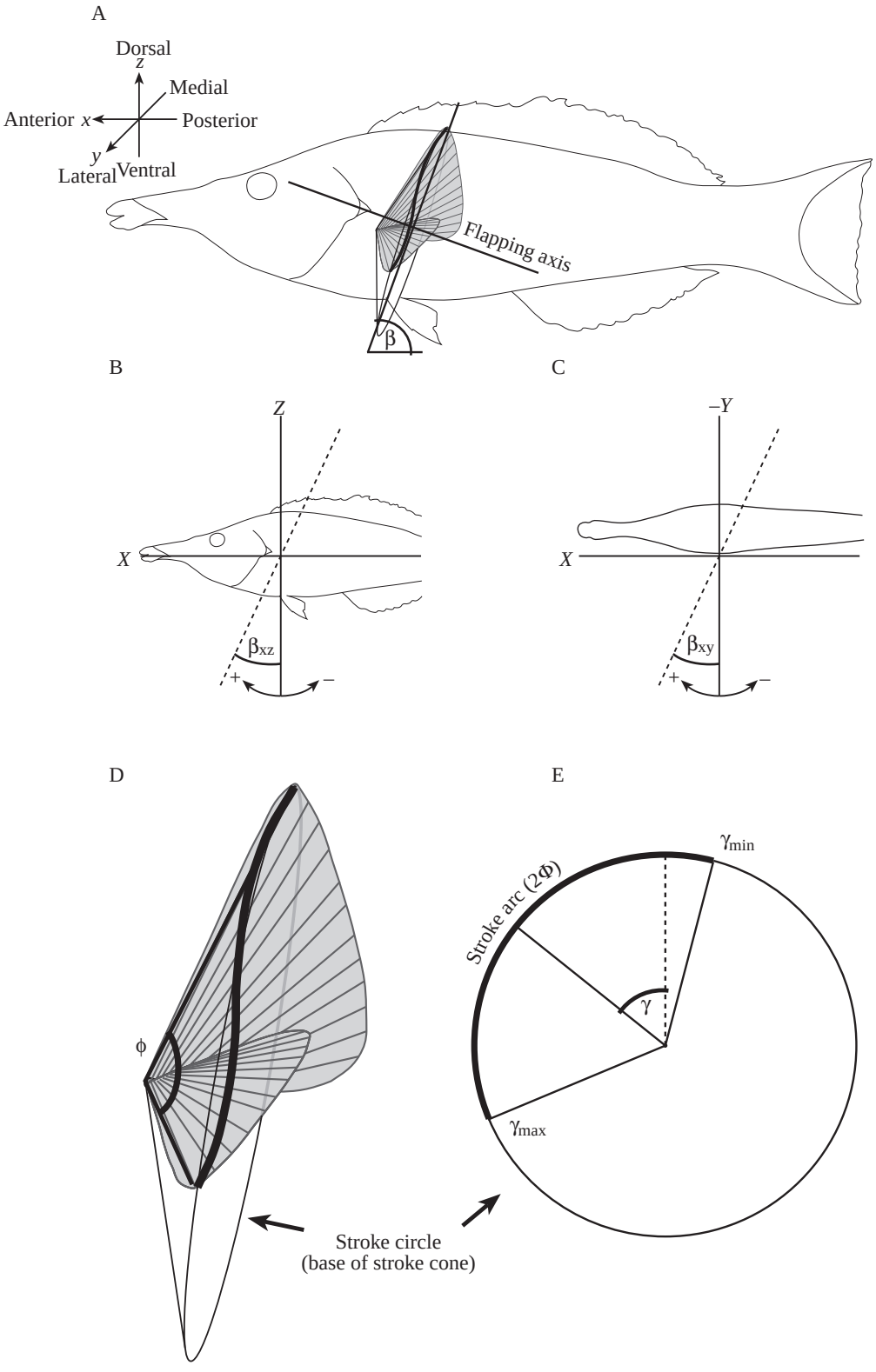

Fig. 3. Geometry of stroke parameters. (A) Geometry of the stroke cone, stroke plane angle, β, and flapping axis. (B) Projection of the stroke plane in lateral view, β_{xz}, indicated by a dashed line. The arrows indicate the sign of the angle, i.e. β_{xz} is positive when the dorsal end of the projection tilts posteriorly. (C) Projection of the stroke plane in dorsal view, β_{xy}, indicated by a dashed line. The arrows indicate the sign of the angle, i.e. β_{xy} is positive when the lateral end of the projection tilts anteriorly. (D) Geometry of the stroke angle, ϕ. The curved line connecting the fin tip at maximum adduction and abduction represents a hypothetical path of travel. (E) Geometry of the instantaneous position of the fin tip (positional angle), γ, the stroke arc and its angle, 2Φ.

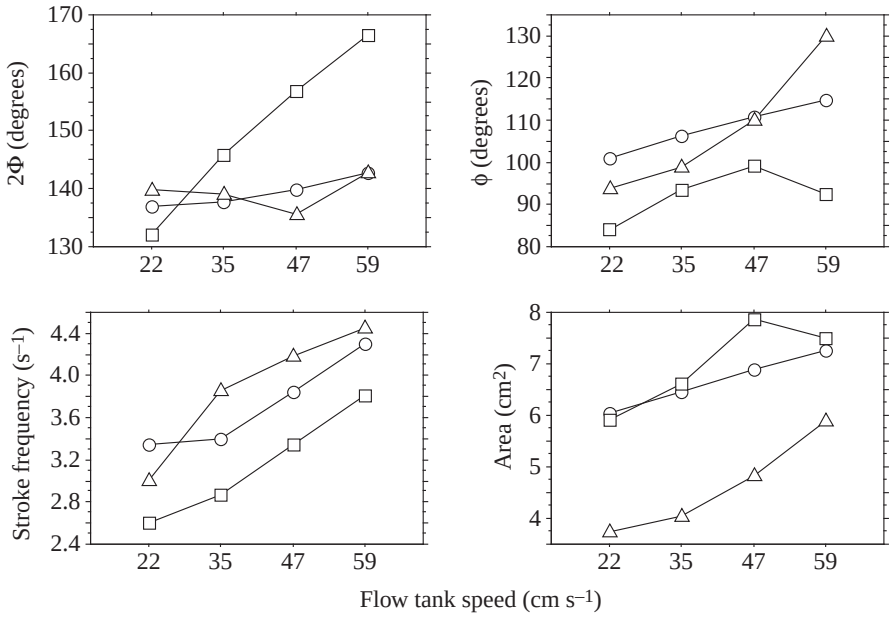

Fig. 4. Changes in stroke parameters with increasing speed. Symbols represent means for each individual at each speed: □ individual 1, △ individual 2, ○ individual 3. Morphological variables for these individuals are given in Table 1. 2Φ, angle of stroke arc, or double amplitude; ϕ, stroke angle (for definitions, see Fig. 3).

actually tilts posteroventrally despite the anteroventral movement of the fin tip during the downstroke.

This paradox is explained by the values of β_{xy} (results not shown), which indicate that the stroke plane is inclined anterolaterally. β_{xz} and β_{xy} are highly correlated (r=0.82, P<0.0001), ranging from anteroventrally inclined planes nearly orthogonal to the anterior–posterior axis in dorsal view (meeting the assumptions of the traditionally defined stroke plane) to vertical or posteroventrally inclined planes with anterolateral orientations in dorsal view. Either of these geometries, or their intermediates, allows the fin tip to travel anteriorly during the downstroke.

The position of the fin-tip marker on the stroke arc is described by a positional angle γ (Fig. 3E). We define the positional angle relative to a vector contained within the intersection of the stroke plane and a sagittal plane through the fin base. γ is positive when the position of the fin marker is lateral to the fin base. γ varies periodically, and we use conventional mathematical definitions to describe the function. The stroke amplitude, Φ, is half the difference between the maximum, γ_{max}, and minimum, γ_{min}, positional angles, the stroke period, T, is the time between adjacent minima, and the stroke frequency, n, is the inverse of the stroke period. We also use γ_{max} to define the time of maximum abduction and γ_{min} to define the time of maximum adduction.

Our definition of stroke amplitude differs from its use in some

Table 2. *Regression statistics for stroke parameters with tank speed as the independent variable*

	1			2			3		
	r	*F*	*P*	*r*	*F*	*P*	*r*	*F*	*P*
β	–0.91	35.50	0.0006*	–0.39	1.63	0.2300	0.49	2.51	0.1516
β_{xz}	0.65	5.00	0.0600	0.87	27.20	0.0006*	0.46	2.06	0.1900
β_{xy}	–0.26	0.50	0.5009	0.85	24.30	0.0008*	0.39	1.43	0.2700
γ	0.11	0.09	0.7688	0.91	46.10	0.0001*	0.85	21.08	0.0018*
2Φ	0.94	49.20	0.0002*	0.04	0.02	0.9038	0.42	1.75	0.2226
ϕ	0.51	2.49	0.1587	0.90	39.71	0.0001*	0.86	22.98	0.0014*
Frequency	0.70	6.61	0.0369	0.89	36.37	0.0002*	0.83	17.49	0.0031
Stroke area	0.72	7.54	0.0287	0.92	49.10	0.0001*	0.91	37.19	0.0003*
Phase lag	0.54	2.05	0.2117	0.28	0.75	0.4104	0.14	0.14	0.7178
%Ad	–0.27	0.55	0.4817	-0.11	0.11	0.7487	–0.10	0.08	0.7903

r is the Pearson product-moment correlation coefficient.
F and *P* are the *F*-statistic and probability of the dependent variable mean squares.
*Significant at table-wise error rate of 0.05 using sequential Bonferroni test (Rice, 1989).
For definitions of symbols see Fig. 3.
%Ad represents the percentage of the stroke cycle accounted for by the adduction phase.
Phase lag is the difference between the leading and trailing edge of the fin.

of the kinematic literature, where it has been defined as the difference between the maximum and minimum positional angles. This difference is actually twice the amplitude, and we refer to it as the double amplitude, 2Φ (equivalent to the degree measure of the stroke arc). In the geometry of the traditionally described stroke plane, 2Φ is the angle between the major axis of the wing at the top and bottom of the stroke. Jensen (1956) referred to this angle as the stroke angle, ϕ. We measured ϕ as the angle between the orientation of the leading-edge ray at maximum abduction and adduction (Fig. 3D). If the leading-edge ray oscillates on the surface of a cone, ϕ will always be less than 2Φ. If the stroke cone collapses into a circle, ϕ will equal 2Φ.

The double amplitude is generally large in *G. varius*, ranging from 125 to 173 °. 2Φ was significantly positively correlated with tank speed in one fish (individual 1) but not in the other two (Table 2). As expected from the geometry of the stroke cone *versus* stroke circle, ϕ values are smaller than corresponding 2Φ values, ranging from 74 to 132 °. In contrast to 2Φ, ϕ increased significantly with swimming speed in individuals 2 and 3 but not in individual 1 (Table 2).

The stroke area is a measure of the area swept by the fin during a half-stroke and is related to the total force generated by the oscillating fins. If the major axis of the fin oscillates in the stroke plane, this area, for both fins, is ϕR_f^2, where R_f is the length of the wing or fin. In *G. varius*, the area swept by both fins, A, varies not only with R_f, but also with the geometry of the stroke cone:

$$A = 4\Phi R_c^2 , \quad (5)$$

where R_c, the radius of the base of the stroke cone, is a function of both R_f and the angle, θ, between the major fin axis, which lies on the edge of the cone, and the flapping axis, which is the central axis of the cone (Fig. 3A):

$$R_c = R_f \cos\theta . \quad (6)$$

A increases significantly with swimming speed in all three individuals (Table 2; Fig. 4), despite the observation that 2Φ does not change significantly in two. This increase is a consequence of the change in the shape of the stroke cone with swimming speed. As speed increases, θ and, consequently, R_c increase, while the height of the stroke cone decreases. Were θ equal to 90 °, R_c would equal R_f and the stroke cone would collapse into the traditionally described stroke circle.

Center of mass kinematics

G. varius oscillates up and down during steady swimming, especially at higher swimming speeds. To quantify the variation in acceleration in both the fore–aft and dorsoventral

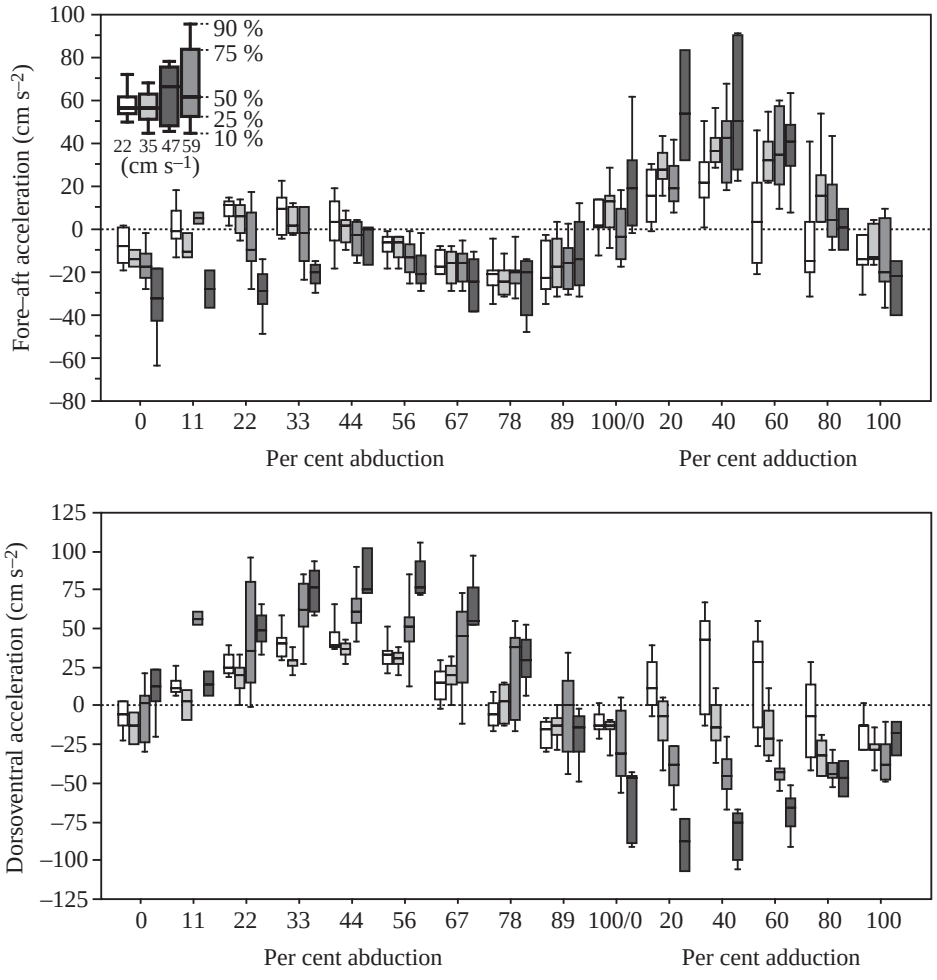

Fig. 5. Distribution of the accelerations of the center of mass in the fore–aft (A) and dorsoventral (B) directions (positive is forward and up). Each box represents the pooled distribution of all sequences and individuals at a given tank speed. Error bars represent standard quartiles, as shown in the inset. Both abduction and adduction in each sequence were standardized independently. Data were binned into ten abduction-phase time classes and six adduction-phase time classes. Both abduction and adduction share the time class at phase transition.

directions throughout the stroke cycle, we smoothed the data using fourth-order central differences, and estimated acceleration components using a five-point 'movable strip' quadratic regression as outlined by Rayner and Aldridge (1985) and described in detail by Lanczos (1988).

The fore–aft acceleration trace (Fig. 5A) presents two acceleration peaks per cycle, one occurring approximately one-third of the way through abduction (0.33Ab or 33 % of the way through abduction) and the second occurring two-fifths of the way through adduction (0.4Ad or 40 % adduction). During abduction, forward (positive) acceleration peaks relatively earlier at low speeds compared with high speeds. During adduction, the peak occurs at the same relative time at all speeds. The magnitudes of the acceleration peaks vary both between abduction and adduction and with speed. The abduction peak is only slightly higher than the adduction peak at low speeds but is substantially higher at high speeds. Median maximal forward acceleration decreases with speed during abduction but increases with speed during adduction.

Acceleration minima occur at or near the phase transitions between abduction and adduction. The adduction minimum, occurring when the fin is maximally adducted, is increasingly negative with increasing speed. The abduction minimum occurs not at maximal fin abduction but at approximately 0.8Ab. Unlike the adduction minima, the abduction minima are similar at all speeds.

The dorsoventral acceleration trace varies considerably among swimming speeds (Fig. 5B). At all speeds, there is a distinct upward (positive) acceleration during abduction occurring at approximately 0.5Ab. Peak accelerations increase with speed at this point of the cycle. During adduction, dorsoventral acceleration has a second upward acceleration maximum at the lowest swimming speed (occurring at 0.4Ad), but a downward acceleration maximum at the highest speed (occurring at 0.2Ad). The acceleration due to gravity of a bird

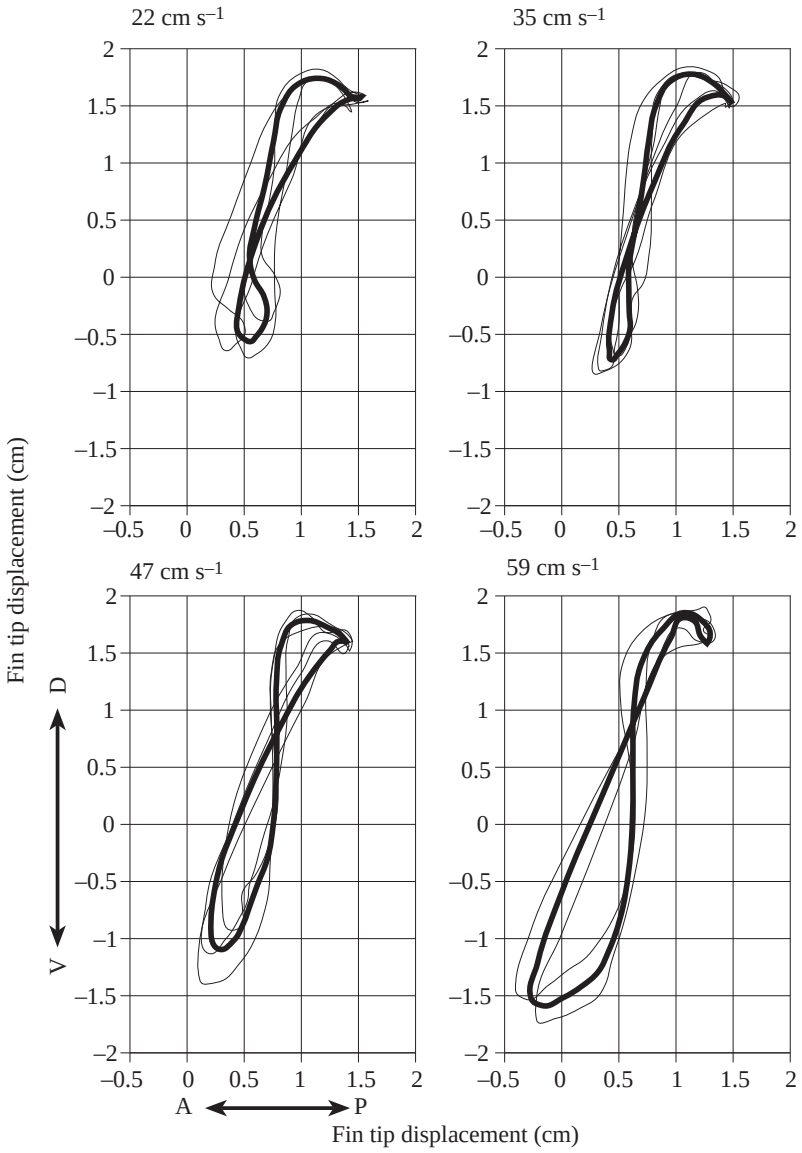

Fig. 6. Left lateral view of fin tip displacement, relative to the body of the fish (the fin base), projected onto the sagittal plane for one individual. The direction of fin-tip movement is counterclockwise around the dorsal loop and clockwise around the ventral loop. Thin lines represent individual sequences. Thick lines represent the mean sequence. The mean sequence was estimated by averaging equally spaced interpolates estimated from a Fourier function fitted to the time-standardized data. Fourier coefficients were estimated using the least-squares method (Hildebrand, 1987). A, anterior; P, posterior; D, dorsal; V, ventral.

wrasse whose weight in water is 2.4 % of that in air (see above) is 24.5 cm s^{-2}, while the peak downward accelerations of the center of mass during adduction at the two highest speeds are in excess of 50 cm s^{-2}.

Stroke geometry

We describe the time-dependent geometry of the fin in both lateral projection (i.e. onto a sagittal or *x,z*, plane) and in the full three-dimensional space of the fish. The fish swims in the positive *x* direction. Lateral motion is along the *y*-axis and up-and-down motion is along the *z*-axis (Fig. 3A).

The trace of the path of the fin tip moving relative to the fin base resembles a thin, inclined or italicized figure-of-eight when projected onto a sagittal plane. The direction of the movement along the figure-of-eight is counterclockwise along the dorsal loop and clockwise along the ventral loop. The traces are similar at all speeds (Fig. 6), except that the dorsal loop appears bigger than the ventral loop at low speeds, whereas the reverse pattern occurs at high speeds. This pattern differs from those of the bluegill sunfish *Lepomis macrochirus*, in which the lateral projection of the fin-tip trace changes dramatically with speed (Gibb *et al.* 1994).

The dorsal side of the figure-of-eight is inclined posteriorly, giving the major axis of the trace an inclination of approximately 70 ° below the horizontal. The base of the pectoral fin is inclined approximately 45 ° below the horizontal; hence, the fin rays do not oscillate in a plane orthogonal to the axis of the fin base.

Relative to the water, displacement of the fin tip resembles a sawtooth pattern when projected onto the *x,z* plane (Fig. 7). This pattern reflects the protraction of the fin during the downstroke and the retraction of the fin during the upstroke. Negative fore–aft displacement of the fin tip occurs during only a small portion (approximately 8 % of the stroke cycle) of the upstroke and only at the lowest swimming speeds (seven of eight sequences digitized at forward speeds of 22 cm s^{-1}, two of eight digitized at swim speeds of 35 cm s^{-1}, and none of the 14 sequences digitized at 47 cm s^{-1} and 59 cm s^{-1}).

We use the figure-of-eight pattern observed in all sequences (Fig. 6) to divide the stroke cycle into four phases. Phases I and II are subdivisions of abduction, while phases III and IV are subdivisions of adduction (see also Fig. 2).

Phase I begins with the fin tip at its maximum posterior position. In this phase, the fin is protracted along the body. Phase II begins with the fin tip at its most superior position. Extension of the fin down and away from the body surface initiates phase II. This motion is led by the distal portion of the fused first and second fin rays and passes distally-to-proximally and anteriorly-to-posteriorly. This has the effect of peeling the fin off the body surface by pulling the fin tip. Following this peel, the fin is depressed and may be slightly protracted or retracted. The tip of the fin is positioned caudal to the fin base throughout this downstroke, giving the pair of fins a swept planform in dorsal view. During the course of the downstroke, the fin is pronated, twisting along its length in a counterclockwise direction (as seen in lateral view). At low velocities, the fin may be maintained near maximum abduction for a short period.

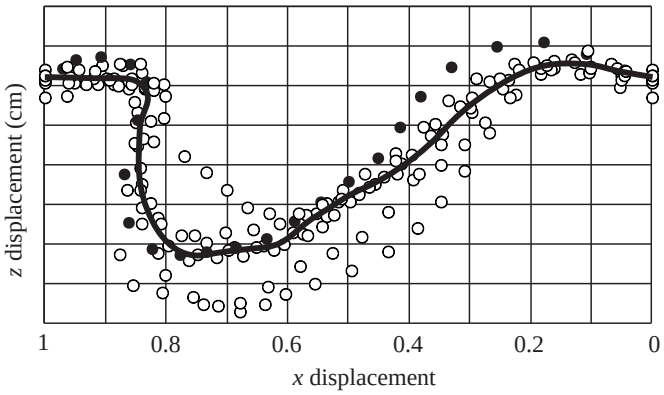

Fig. 7. Left lateral view of fin tip displacement (projected onto the *x,z* plane), relative to the water, for all sequences and individuals at 22 cm s^{-1}. Individual sequences, represented by the open circles, are composed of equally spaced interpolates estimated from a Fourier function fitted to the time-standardized data. Fourier coefficients were estimated using the least-squares method (Hildebrand, 1987). A single sequence is highlighted by the filled circles. The thick line represents the median path for all sequences.

In phase III, the fin is supinated, protracting and elevating the leading edge and causing the fin to twist in a direction opposite to that in phase II. In phase IV, the fin is rapidly retracted and elevated to the initial phase I position. Supination continues at the beginning of phase IV, causing the distal portion of the fin to have a nearly vertical orientation.

The vertical oscillation and dynamic twisting of the fin causes the chords between the markers to heave (translate) and pitch (rotate) throughout the stroke cycle. Projections of the proximal and distal chords on a sagittal plane (Fig. 8) illustrate time-dependent changes in the position (due to heave) and orientation (due to pitch) of the proximal and distal chords. Time-dependent changes in pitch for the proximal chord (Fig. 8A) are fairly simple because of the very small displacement of the proximal trailing-edge marker throughout the stroke cycle. At the start of phase I, the chord has a high positive, or nose-up, pitch at all speeds. During the downstroke (phase II), the pitch gradually decreases, reaching small negative, or nose down, values at higher speeds. In phases III and IV, the pitch gradually increases with a pattern that is simply the reverse of that in phases I and II.

In contrast to that of the proximal chord, the pattern of change in pitch of the distal chord differs appreciably between the abductive and adductive phases (Fig. 8B). The leading-edge fin ray begins the downstroke (phase II) while the trailing-edge fin ray is still elevating and protracting, and is approximately half-way through phase II when the trailing edge begins depression. This delay in the trailing edge results in the distal chord attaining negative pitch midway through phase II at all speeds. The distal chord has a distinct convex

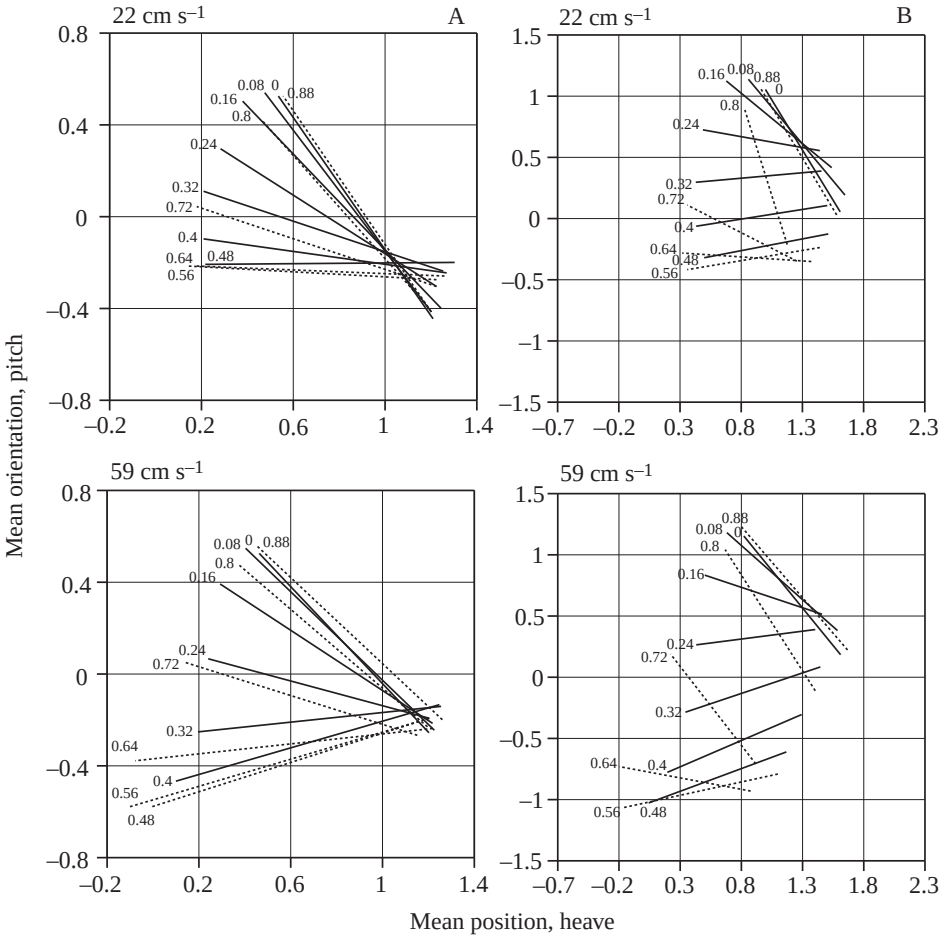

Fig. 8. Left lateral view of changes in mean position (heave) and mean orientation (pitch) of (A) proximal and (B) distal chords for a single individual over all trials at 22 cm s^{-1} and 59 cm s^{-1}. Mean values were estimated from the positions of the interpolates estimated from a Fourier function fitted to the time-standardized data. Fourier coefficients were estimated using the least-squares method (Hildebrand, 1987). The numbers identify the standardized time (percentage of stroke period) associated with the neighboring chord. The solid line represents the chord during abduction, the broken line represents the chord during adduction.

upward bend during this part of the stroke cycle. During the second half of the downstroke, the distal chord reaches higher negative pitch at higher speeds. The leading edge protracts and elevates in phase III while the trailing edge is still depressing, producing a small positive pitch. In phase IV, the trailing edge reaches maximum protraction at approximately the time that the leading edge has rotated half the distance back to the starting location of phase I. The distal chord, therefore, reattains a high positive pitch during this phase. The highest positive pitch occurs in fish swimming at the lowest swimming speed. During phase IV, the distal chord presents a distinct convex-downward bend.

Undulation

Inspection of heave and pitch of the fin chords suggests that the leading and trailing edges are out of phase, with the trailing edge lagging behind. This phase difference reflects an undulatory wave passing from the leading to the trailing edge. To illustrate the phase lag, we compared the instantaneous positional angles, γ, of the leading-edge distal marker (γ_{le}) and trailing-edge distal marker (γ_{te}) (Fig. 9). A positional vector is the radian vector from the center of the stroke circle to the projection of the coordinates of the distal marker onto the stroke plane (Fig. 3E). γ is the angle between the positional vector and a dorsoventral radian vector (Fig. 3E). In this geometry, γ measures the magnitude of abduction. Angles near 0 ° indicate a leading- or trailing-edge fin ray that is near maximum adduction, while angles greater than 90 ° indicate a leading- or trailing-edge fin ray that is near maximum abduction. It is important to note, however, that the fin rays do not rotate within the stroke plane and, thus, γ measures the degree of abduction of the hypothetical position vector.

The phase lag between the leading and trailing edges at the distal chord is apparent from the distribution of these positional angles (Fig. 9). Minimum γ_{le}, by definition, occurs at 0Ab, while minimum γ_{te} occurs between 0.11Ab and 0.22Ab. Maximum γ_{le}, by definition, occurs at 0Ad while maximum γ_{te} occurs between 0Ad and 0.2Ad.

The distribution of positional angles in Fig. 9 suggests a phase lag of between 10 and 20 % of the stroke cycle. To quantify the phase lag more rigorously, we estimated the phase lag for each sequence as the difference in time between maximum γ_{te} and maximum γ_{le}. The mean phase lag across all sequences, fish and speeds is 19.2 ° (0.33π). We found no correlation between phase lag and swimming speed (Table 2).

The computation of this phase lag allowed us to compute a rough estimate of wave speed, V_w, at the distal chord:

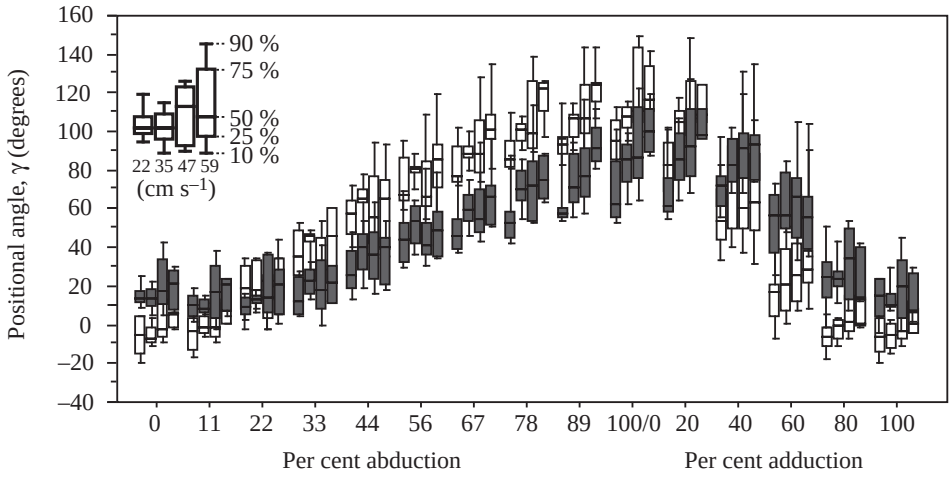

Fig. 9. Distribution of positional angle, γ, for the leading-edge distal marker (open boxes) and trailing-edge distal marker (shaded boxes). Both abduction and adduction in each sequence were standardized independently. Data were binned into ten abduction-phase time classes and six adduction-phase time classes. Both abduction and adduction share the time class at phase transition. Speeds increase from left to right in the inset for each group of four. Error bars represent standard quartiles, as shown in the inset.

$$V_w = \frac{c\pi n}{\delta}, \quad (7)$$

where c is distal chord length, n is stroke frequency and δ is the phase lag. Wave speed increased significantly from 24.4 to 52.5 cm s^{-1} (F=12.1, P=0.0018). It is interesting to note that wave speed was higher than swimming speed at the two lowest test speeds but lower than swimming speed at the two highest test speeds.

Velocity and acceleration components

The velocity of the fin relative to the water depends on both the velocity due to the fin flapping and the swimming speed of the fish. To estimate the components due to fin flapping, we used a four-point quadratic regression to approximate the function describing fin displacement at each time. Velocities were estimated by differentiating the quadratic function. We used a four-point regression as inspection of time–displacement plots of markers revealed that the sampling frequency (60 Hz) was too low to justify regression through five points. A four-point regression is asymmetric about the point of interest; the regression may include either the two points prior to or the two points following the focal point. We used the average of the estimates computed from the two asymmetric regression functions.

We computed the instantaneous velocity of the tip marker and the leading-edge distal marker due to fin flapping. To these, we added the velocity of the center of mass to give the resultant velocity of the marker relative to the water, v_{res}. Reversing the sign of v_{res} gives an estimate of the resultant flow velocity over the fin. This estimate, $-v_{res}$, ignores the induced velocity component. Induced velocity can be understood by thinking of the flapping fins as a helicopter rotor. Lift in a helicopter rotor is a reaction force resulting from the rotor accelerating a mass of air past the blades. The induced velocity is the additional velocity due to this increased momentum.

Induced velocity is difficult to measure directly (but see Blake, 1979*b*). Application of detailed hydrodynamic models estimating induced velocity (Archer *et al.* 1979; Phlips *et al.* 1981; Azuma *et al.* 1985; DeLaurier, 1993) was beyond the scope of the present analysis. Induced velocity is often estimated using momentum theory (Osborne, 1951; Weis-Fogh, 1973; Norberg, 1976). The assumptions of momentum theory, that induced velocity is constant both over time and along the fin, are grossly violated for a flapping fin. Nevertheless, we used momentum theory to obtain a rough estimate of the error of ignoring induced velocity. The momentum theory estimate of induced velocity is approximately 6 % of v_{res} at the mid half-stroke and 12 % of v_{res} at full abduction and adduction. The maximum difference in direction (i.e. if the induced velocity were normal to v_{res}) at the mid half-stroke is approximately 3.4 °, while at the end of each half-stroke it is 6.8 °. Given the caveats of applying momentum theory, in combination with the relatively small influence of the induced velocity on the direction and magnitude of the resultant stream, we have chosen to ignore the induced velocity component of the resultant stream.

In Fig. 10, we illustrate the fore–aft component of v_{res} for both the fin tip and the leading-edge distal marker. The downstroke has an early peak at approximately 0.22Ab, reflecting the initial protraction during phase I. A trough occurs between 0.44Ab and 0.67Ab due to the largely ventral, or even posteroventral, translation of the fin relative to the fish. A second peak occurs at around the transition from downstroke to upstroke, reflecting the protraction occurring in phase III. Finally, the rapid retraction of the fin during the upstroke results in a marked trough occurring between 0.4Ad and 0.6Ad. It is important to note that the tip marker, but not the distal marker, attained negative velocities at this point in the stroke cycle in individuals swimming at the lowest forward speeds but not at the higher forward speeds. Thus, the fin moved backwards faster than the fish moved forwards only at the lowest forward speeds, only for the distal portion of the fin and only for a short period. We should note that the reduction in the fore–aft component of fin velocity midway through adduction is not associated with a decreased flow over the fin.

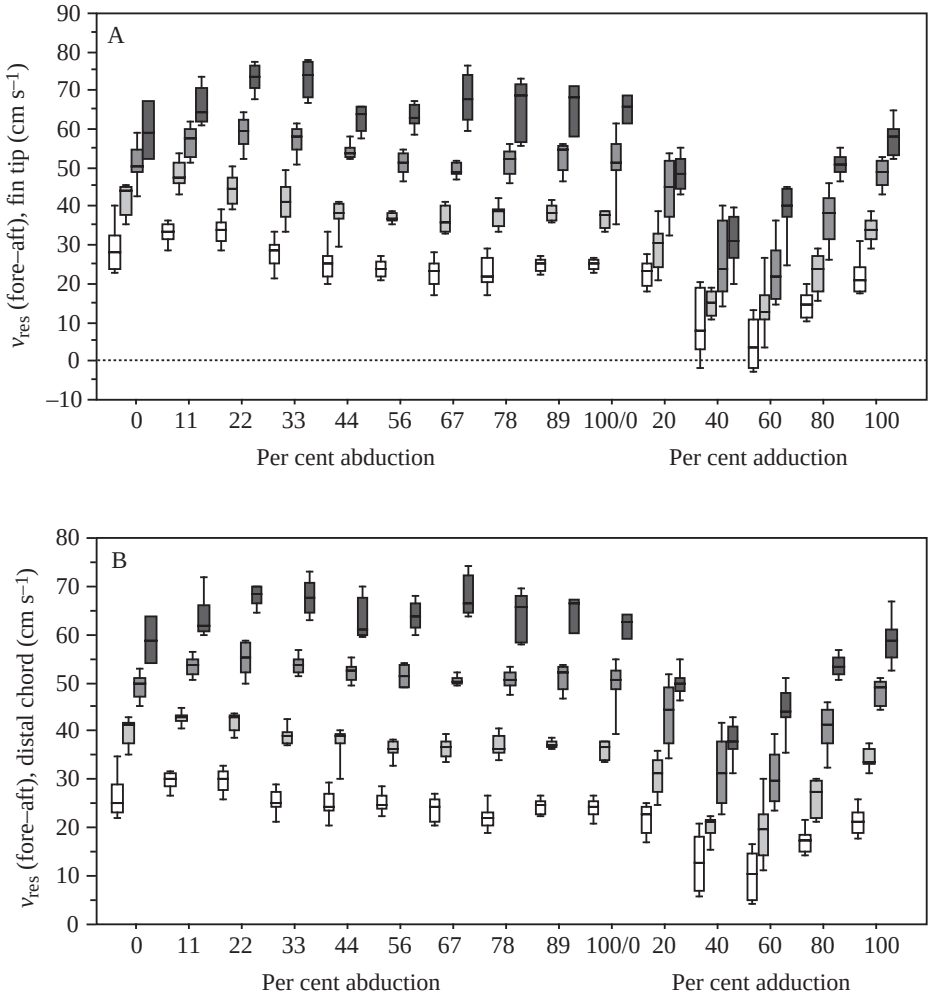

Fig. 10. Distribution of the fore–aft velocity component at the fin tip (A) and distal (B) marker. Values are positive in the direction of swimming. Negative velocities indicate that the fin is moving backwards faster than the fish is moving forwards. Sequence standardization and box plots are as in Fig. 5. v_{res} is the resultant velocity of the marker relative to the water.

On the contrary, the peak magnitude of v_{res} occurs between 0.4Ad and 0.6Ad (results not shown).

An oscillating fin accelerates and decelerates a mass of water, generating added-mass forces that can contribute to thrust (Daniel, 1984). Added-mass forces are proportional to $-(dv_n/dt)$, where t is time and v_n is the component of flow velocity normal to the fin.

$$v_n = v_{res}\cos\psi\,. \tag{8}$$

ψ is the angle between the resultant stream and the vector, **n**, normal to the fin at the relevant chord. **n** is found by:

$$\mathbf{n} = \mathbf{m}\times\mathbf{c}\,, \tag{9}$$

where, **m** is the vector from the base of the fin to the tip of the major axis and **c** is the chord vector, centered at the leading edge.

Profiles of the fore–aft and dorsoventral components of dv_n/dt for the leading-edge distal marker are illustrated in Fig. 11. We used the distal fin chord (see Fig. 1) to estimate the orientation of the fin near the tip (equation 9). A small negative fore–aft acceleration peak occurs during the first half of the downstroke, but remarkably trivial fore–aft accelerations characterize the second half. By contrast, during the upstroke, a second small negative fore–aft acceleration peak is rapidly followed by large positive accelerations that peak at approximately 0.6Ad. Dorsoventral accelerations are largely positive during the downstroke, although a small negative peak occurs between 0.33Ab and 0.44Ab. A large positive dorsoventral acceleration peak occurs at the transition from abduction to adduction (0Ad). Finally, a large negative dorsoventral acceleration occurs midway through the upstroke.

Angles of attack

We estimated two angles of attack. The morphological angle of attack, α_m, is the angle between the chord of interest and a frontal plane (Fig. 12).

$$\alpha_m = (\pi/2) - \cos^{-1}\left(\frac{(\mathbf{i_x}\times\mathbf{i_y})\cdot\mathbf{c}}{|\mathbf{c}|}\right), \tag{10}$$

where $\mathbf{i_x}$ and $\mathbf{i_y}$ are unit vectors in the positive x and y directions, respectively, and **c** is the vector from the leading-edge chord marker to the trailing-edge chord marker (centered at the leading-edge chord marker). The local stream angle, α_{res}, is the angle between the resultant stream vector, $-\mathbf{v_{res}}$, and a frontal plane (Fig. 12):

$$\alpha_{res} = (\pi/2) - \cos^{-1}\left(\frac{(\mathbf{i_x} \times \mathbf{i_y}) \cdot \mathbf{v_{stream}}}{|\mathbf{v_{stream}}|}\right), \quad (11)$$

where $\mathbf{v_{stream}}$ is the local stream vector. The proximal chord maintains a positive α_m through most of the first half of the downstroke (Fig. 13A). At the lowest forward speed, a negative α_m was achieved in approximately half of the sequences. Maximum negative α_m, generally occurring from 0.8Ab to 0.9Ab, increased with forward speed. At the two highest forward speeds, a negative α_m was generally maintained until 0.2Ad.

The distal chord achieves a negative α_m sooner in the stroke cycle (at approximately 0.44Ab) than the proximal chord (Fig. 13B). Negative α_m values occur at all speeds, but their magnitude increases with speed. At each speed, the maximum negative α_m is greater for the distal chord than for the proximal chord. During the upstroke, a positive α_m is rapidly achieved at approximately 0.4Ad.

Local stream angles were estimated for the fin-tip marker and the leading-edge marker of the distal chord (Fig. 14). At the fin tip, α_{res} is initially positive, corresponding to the elevation of the fin during phase I. With the initiation of the downstroke, α_{res} achieves and maintains negative angles until 1.0Ab. Maximum negative angles during the downstroke are approximately −40 °. During the upstroke, α_{res} becomes rapidly positive at the fin tip and reaches peak positive angles at 0.4–0.6Ad. At the lowest forward speed, peak positive angles are sometimes greater than 90 °. The pattern of α_{res} for the distal chord is similar to the pattern at the fin tip. In general, peak negative and positive angles are smaller than those occurring at the fin tip (reflecting the lower flapping velocity at the distal chord compared with that at the fin tip). In contrast to the fin tip, α_{res} at the distal chord is almost never greater than 90 ° during any part of the upstroke, even at the lowest forward speed.

The hydrodynamic angle of attack, α_h, is given by $\alpha_m - \alpha_{res}$. This angle (Fig. 14) is positive throughout the first two-thirds of the downstroke and negative for the last quarter of the downstroke and the first half of the upstroke.

Discussion

Members of the families Labridae, Scaridae, Embiotocidae, Acanthuridae and Gasterosteidae swim at relatively high speeds ($\gg 1\ TL\ s^{-1}$) employing only their pectoral fins. Despite the common use of pectoral fin locomotion among fishes, only

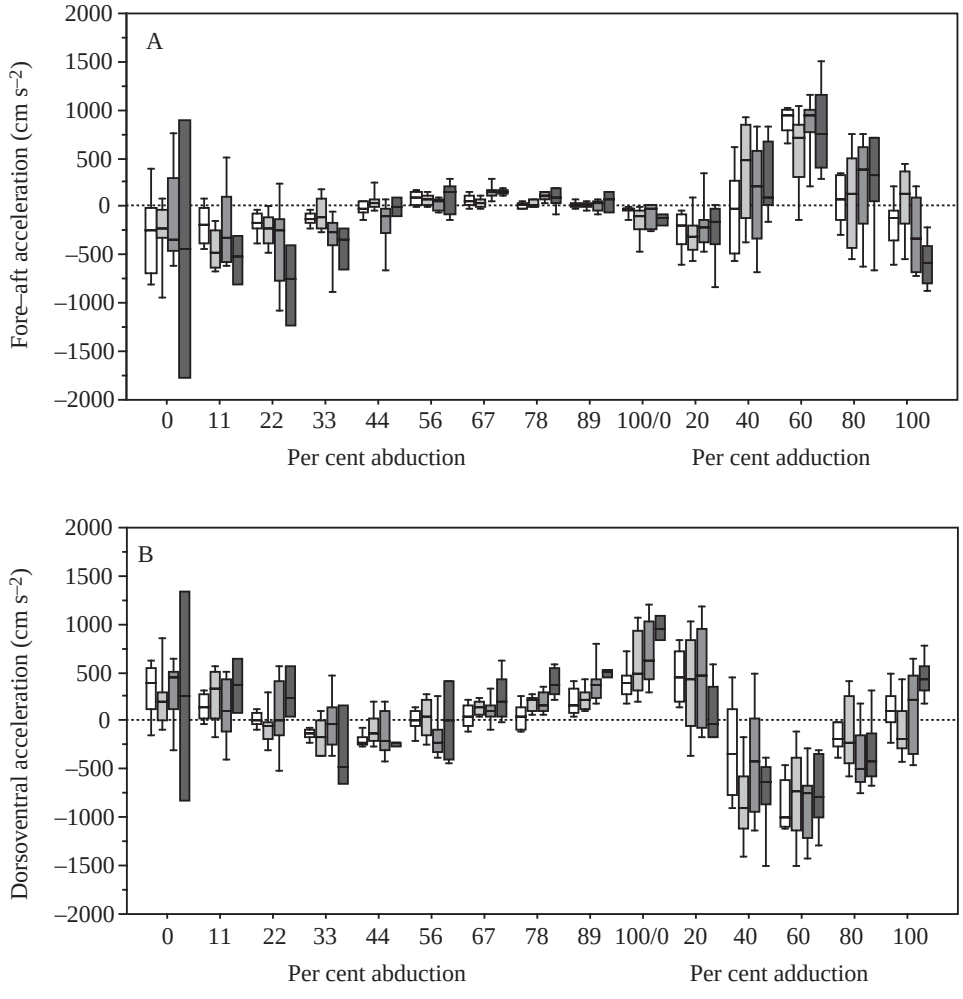

Fig. 11. Distribution of fore–aft (A) and dorsoventral (B) components of normal acceleration (positive is forward and up) of the leading-edge distal marker. Sequence standardization and box plots are as in Fig. 5.

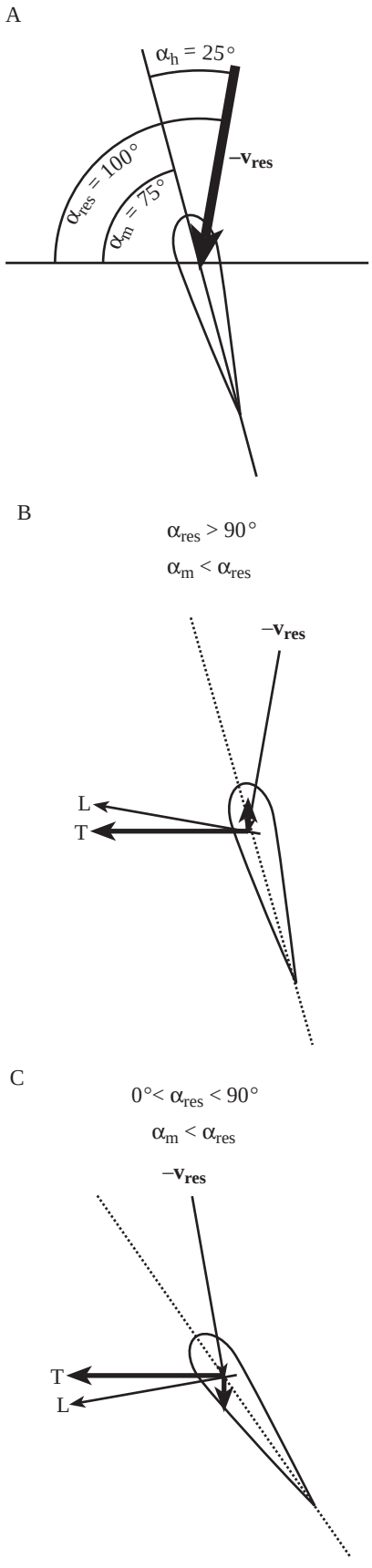

two reports on pectoral fin kinematics in fishes swimming at high speeds have been published: Webb's (1973) investigation of the shiner surfperch *Cymatogaster aggregata* (Webb, 1973) and Drucker and Jensen's (1996) work on the striped surfperch *Embiotoca lateralis*. Both Webb (1973) and Drucker and Jensen (1996) concentrated on the effects of increased swimming speed on stroke parameters. Our data on *Gomphosus varius* highlight for the first time the kinematic details of fin motion in a fish employing flapping aquatic flight across a wide range of speeds.

Stroke parameters

To increase swimming speed, a fish must modify its propulsive kinematics in order to generate the extra thrust required to overcome the increased drag on the body. Increased flapping frequency, stroke amplitude or both are common mechanisms of generating increased thrust in many paired-appendage propulsors. In the present study, flapping frequency increases with tank speed in all individuals tested. An increase in flapping frequency both maintains an appropriate direction of the resultant stream vector to generate a thrust component of hydrodynamic lift and increases any contribution from the acceleration reaction. Thrust increases with the volume of water accelerated by the flapping fins. *G. varius* controls this volume by either increasing stroke amplitude or 'flattening' the stroke cone.

It is difficult to compare our measures of fin excursion, ϕ and 2Φ, with those of previous studies because our angles reflect the actual three-dimensional displacement of the fin tip while all previous studies report only the projection of the displacement onto a single plane (Blake, 1979*a*; Geerlink, 1983; Archer and Johnston, 1989; Gibb *et al.* 1994; Drucker and Jensen, 1996). In fishes that abduct the leading edge along a largely horizontal stroke plane, a measure of amplitude from a dorsal view (as in Blake, 1979*a*; Archer and Johnston, 1989) will closely approximate a three-dimensional measure. The leading edge of the fin rotates by 120–140 ° in the frontal plane of *Coris formosa* (Figs 2, 4 in Geerlink, 1983) but only by 90 ° in *Cymatogaster aggregata* (Webb, 1973). In *G. varius*, leading-edge rotation within the frontal plane increases with swimming speed (as can be deduced from Fig. 6) and only regularly exceeds 90 ° (when the tip attains negative *x* values) at 59 cm s^{-1}. Rotation in the frontal plane is somewhat misleading for the bird wrasse. Because of the largely

Fig. 12. Hypothesis of resultant forces acting on the distal fin. (A) Explanation of angles. α_m, morphological angle of attack; α_h, hydrodynamic angle of attack; α_{res}, resultant angle of attack ($\alpha_{res}=\alpha_m+\alpha_h$); $-\mathbf{v_{res}}$, resultant stream vector. (B) When the fin chord translates backwards faster than the fish is moving forwards, the resultant stream vector has an angle of greater than 90 ° to a positive *x* vector. If α_h is negative, lift will have both forward and upward components. (C) When the fin chord translates backwards slower than the fish is moving forwards, the resultant stream vector has an angle of less than 90 ° to a positive *x* vector. If α_h is negative, lift will have both forward and downward components. L, lift; T, thrust.

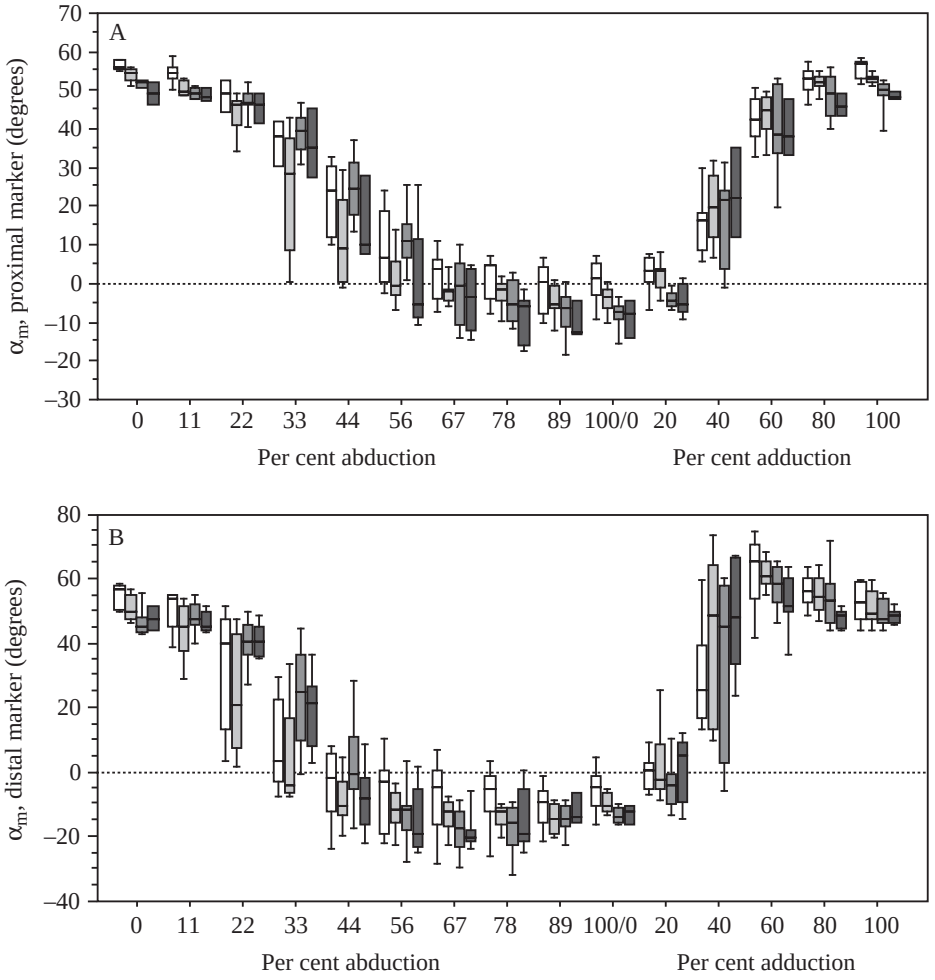

Fig. 13. Distribution of morphological angle of attack, α_m, for (A) the proximal and (B) the distal chords of the fin (see Fig. 1). Sequence standardization and box plots are as in Fig. 5.

dorsoventral motion of the pectoral fin, large rotations of the leading edge in the frontal plane are associated with only very small forward displacements of the fin tip.

While amplitude increased monotonically in *G. varius*, it increased asymptotically in two embiotocids, *Cymatogaster aggregata* and *Embiotoca lateralis* (Webb, 1973; Drucker and Jensen, 1996). Drucker and Jensen used the difference between the maximum and minimum dorsoventral positions of the fin tip as a measure of amplitude (as did Gibb *et al.* 1994). The mapping between angular displacement and a rectangular proxy is nonlinear. An asymptotic relationship between rectangular amplitude and speed is expected even if the angular amplitude relationship is linear (as long as the amplitude exceeds approximately 160 ° at the high speeds). Nevertheless, the long plateau present in Fig. 3 of Drucker and Jensen (1996) suggests that the flattening results largely from the angular amplitude reaching its asymptotic value rather than from a mapping artifact. If a plateau is expected in fishes swimming at speeds approaching the maximum sustainable speed using only the pectoral fins (U_{pc} of Drucker and Jensen, 1996), the absence of a plateau in the *G. varius* curves probably reflects the fact that the highest speeds attained in this study are less than two-thirds of the estimated U_{pc}.

Frequency and amplitude are related by a non-dimensional frequency parameter, the Strouhal number *St* (Triantafyllou *et al.* 1993):

$$St = \frac{n\Delta}{\bar{U}_{fish}}, \quad (12)$$

where n is stroke frequency, A is the maximum displacement of the fin tip and $\bar{V}$ is the mean forward velocity of the fish. *St* is a measure of the wake geometry behind an oscillating fin and, therefore, both thrust and mechanical efficiency are causally associated with it (Triantafyllou *et al.* 1993). Theoretical modeling and experimental results indicate that optimal efficiency occurs when *St* lies in the range 0.25–0.35 (Triantafyllou *et al.* 1993). Indeed, *St* for many fishes and cetaceans swimming at or near peak sustained speeds, at *Re* values of 10^4–10^6, was in the range 0.25–0.35 (Triantafyllou *et al.* 1993). In the bird wrasse, *St* decreased asymptotically with swimming speed, with mean values of 0.54 at 22 cm s^{-1} and 0.31 at 59 cm s^{-1}. The estimated *St* at 6 *TL* S^{-1} (near the measured maximum sustained swimming speed for bird wrasses of the size in this study) is 0.27.

A wave propagating along a median or pectoral fin generates both resistive and reactive forces, and many fishes employ a variation of this mechanism for hovering and for forward and

backward swimming (Breder, 1926; Harris, 1937; Lighthill, 1969, 1975; Lighthill and Blake, 1990; Lindsey, 1978; Blake, 1979*b*; Daniel, 1988; Arreola and Westneat, 1996). A dorsoventrally flapping pectoral fin can potentially generate thrust by propagating a wave from the leading to the trailing edge, even though the fin, as a whole, has no fore–aft oscillation (Daniel, 1988). As discussed above, pitching the fin nose-downward during the downstroke and nose-upward during the upstroke effectively propagates a wave from the leading to the trailing edge. The average magnitude of the phase difference at peak abduction indicates that only 10 % of a full wave is present at any one time on the distal chord. Our estimates of the speed of this wave are approximate but suggest that, at low test speeds, backward propagation of the wave exceeds the forward speed of the fish.

Unlike the nearly constant, small (19 °) phase lag between the leading and trailing edges observed in the bird wrasse, the phase lag in *C. aggregata* differed markedly with speed (Webb, 1973). At low speeds, the phase lag (type A motion in Webb, 1973) was close to 180 °. At higher speeds (type B motion in Webb, 1973), the phase lag was only 36 ° and thus resembles the more rigid flapping of the bird wrasse fin. The large phase lag in *Coris formosa* swimming at slow speeds, of 90–180 ° (Geerlink, 1983), resembles type A motion of *C. aggregata*.

We expect large differences in the stroke plane angle between fishes using a drag-based or lift-based mode. Unfortunately, stroke plane angles have not been measured for the pectoral fins of any fish prior to the present study. Fig. 1 in Drucker and Jensen (1996) suggests that *Embiotoca lateralis* has a steep stroke plane, similar to that of the bird wrasse. Blake (1983*b*) mentioned that Webb's films of *Cymatogaster*

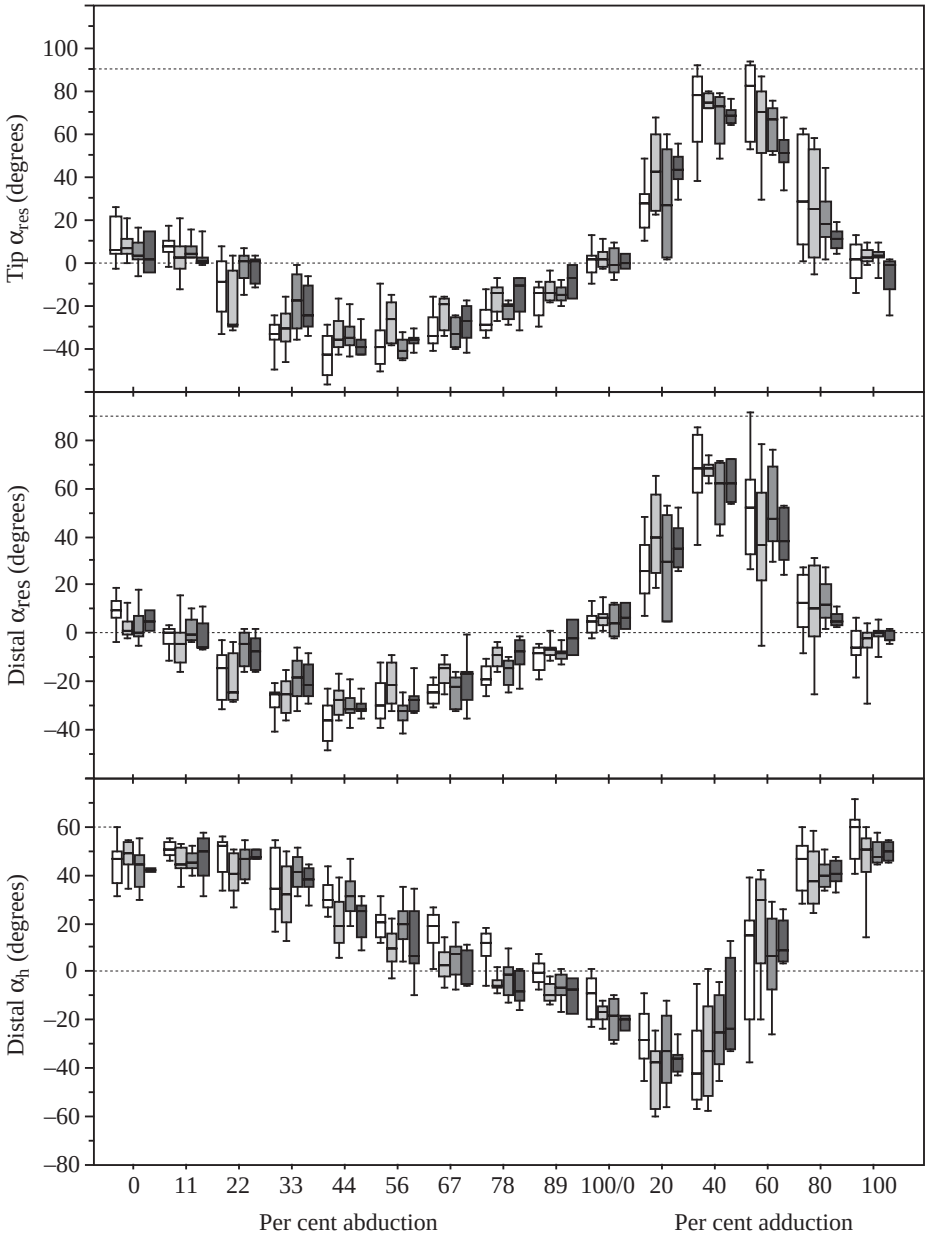

Fig. 14. Distribution of local stream angle, α_{res}, at the tip marker (top panel) and distal leading-edge marker (middle panel) and hydrodynamic angle of attack, α_h, at the distal leading-edge marker (bottom panel). Sequence standardization and box plots are as in Fig. 5.

aggregata indicate a stroke plane angle of approximately 70° (or 20° below the horizontal). This estimate seems unusually flat for a lift-based swimmer; perhaps Blake's estimate is from a low swimming speed, when *C. aggregata* employs type A motion (Webb, 1973), which may be more drag-based.

Geerlink (1983) noted that the fin stroke of *Coris formosa* swimming at slow speeds (0.4–0.8 $TL\,s^{-1}$) differed from the rowing stroke of *Pterophyllum eimekei* (Blake, 1979*a*, 1980) in the distinctly downward movement of the leading edge during abduction. But the leading edge of a fin has to depress during abduction in a rowing stroke in order for the fin to feather properly. Illustrations of the pectoral fin in *C. formosa* show the leading edge of the fin rolling over the trailing edge during the first half of abduction (Geerlink, 1983). This roll, reflecting the depression of the leading edge while the trailing edge is still elevating, helps to feather the fin rapidly during abduction (note that with some downward motion of the fin, as a whole, during abduction, a perfectly feathered fin is pitched nose-downward, as illustrated for *C. formosa*).

The adduction phase also differs considerably between *G. varius* swimming at high speeds and *Coris formosa* swimming at low speeds. In *C. formosa*, the fin tip maintains negative fore–aft velocities for much of adduction (Geerlink, 1983), while the fin in *G. varius* attains negative velocities for only a very short period and only at the lowest forward speeds. The long period of negative fin-tip velocities during adduction suggests that *C. formosa* employs a drag-based mechanism of thrust generation, at least at slow speeds. All wrasses observed in our laboratory can achieve and maintain relative swimming speeds much greater than those analyzed for *C. formosa*, and it is assumed that *C. formosa* can as well. Whether *C. formosa* employs a more lift-based mechanism at higher speeds remains to be investigated. The bird wrasse does not use a more drag-based mechanism at the lower speeds investigated in this study and, perhaps as a consequence, cannot swim steadily at low relative speeds (less than 1.2 $TL\,s^{-1}$).

Hydrodynamic inferences

The largely dorsoventral motions of the flapping fins in *G. varius* suggest that hydrodynamic lift due to a net circulation around the fins is the major steady mechanism for generating thrust at the center of mass during sustained swimming at all speeds. From kinematic patterns of the center of body mass, we have inferred three hydrodynamic features of the bird wrasse fin stroke. (1) A small thrust peak occurs midway through abduction (downstroke), while a larger thrust peak occurs midway through adduction (upstroke). (2) An upward force peak occurs during the downstroke. The magnitude of this peak increases with swimming speed. (3) The dorsoventral force peak occurring during the upstroke is speed-dependent. At slow speeds, a small upward force occurs. At higher speeds, a downward force peak occurs. The magnitude of the downward force peak increases with speed. The magnitude of this downward peak at the two higher speeds exceeds the downward acceleration due to gravity and, therefore, reflects downward forces generated by the adducting fins.

Steady-state aerodynamic properties of wings over a range of attack angles and velocities can be directly measured using a force balance and a wind-tunnel (Jensen, 1956; Vogel, 1967; Zanker and Götz, 1990). In a quasi-steady analysis of flapping wing propulsion, these aerodynamic properties are used to estimate forces acting along the length of the wing at each instant of the wingbeat cycle (Jensen, 1956; Vogel, 1967; Norberg, 1976; Azuma *et al.* 1985; Zanker and Götz, 1990; Dudley and Ellington, 1990; Wilkin and Williams, 1993). The major assumption of a quasi-steady analysis is that the forces acting on a flapping wing section at any instant are similar to the steady-state forces acting on a wing section at the same angle of attack and flow velocity.

A qualitative quasi-steady analysis based on the orientation of the fin chords and the resultant stream suggests steady hydrodynamic mechanisms that could account for the inferred dynamics of the center of mass.

The resultant stream attains an upward component at the beginning of phase II (0.22Ab). At this time, the fin is rapidly pronating, allowing the distal fin to maintain a small positive hydrodynamic angle of attack until approximately 0.67Ab (Fig. 14). The geometry of the resultant stream (Fig. 14) and fin pitch (Fig. 13) at the distal chord during the first half of the downstroke should create a lift force with large dorsal and small forward components. This inference is supported by the acceleration profile of the center of mass: the smaller of the fore–aft peaks occurs between 0.33 and 0.44Ab, while a large dorsal acceleration peak occurs at 0.44Ab (Fig. 5).

During the upstroke, the resultant stream velocity vector has a positive fore–aft component only when the tangential velocity of the fin in the backward direction is greater than the forward speed of the fish. This positive *x* component occurs for the fin tip in most of the sequences filmed at 22 $cm\,s^{-1}$, very few of the sequences at 35 $cm\,s^{-1}$ and none of the sequences at the two highest forward speeds. By contrast, at the level of the distal chord, very few of the sequences, even at the lowest forward speed, present positive fore–aft velocities.

A positive *x* component of the resultant stream vector has interesting implications for the kinematics of the center of mass. Given both a positive *x* component and a small negative hydrodynamic angle of attack, any generated circulatory lift will have both a forward and an upward component (Fig. 12). However, a negative *x* component combined with a small negative hydrodynamic angle of attack results in a forward and downward component (Fig. 12). The difference in sign in the *x* component of the local stream between the lowest swimming speed and the three higher swimming speeds is, therefore, the likely cause of the upstroke peak in positive fore–aft acceleration at the center of mass in the lowest speed trials (Fig. 5), a peak that does not exist at higher swimming speeds.

The much more vertically oriented resultant velocity vector during the upstroke compared with the downstroke (Fig. 14) suggests that thrust forces are much greater during the upstroke. Again, this hypothesis is supported by the kinematics of the center of mass (Fig. 5), which indicates that the major thrust peak occurs at approximately 0.4Ad. The asymmetry

between the orientation of the resultant stream between the downstroke and the upstroke suggests that the sum, or impulse, of the upward forces during the downstroke is greater than the sum of the downward forces during the upstroke. This net upward hydrodynamic force for the stroke as a whole should be equal in magnitude to the downward force due to gravity on the negatively buoyant bird wrasse.

The positive *x* component of the resultant stream during a small portion of the upstroke at the slowest forward speeds indicates also that the hydrodynamic drag generated during this period contributes to thrust at the center of mass. While this is a drag-based mechanism of thrust generation, the bird wrasse should not be considered a 'drag-based' swimmer, even at slow swimming speeds.

Unsteady mechanisms

There are, of course, potential problems with this qualitative quasi-steady hydrodynamic inference. The efficacy of a quasi-steady analysis to estimate the actual force profile on an oscillating wing diminishes as the reduced frequency parameter, *k* (see Table 1 for a definition), increases (Spedding, 1992, 1993). *k* is essentially the ratio of the motion of the wing due to oscillation to the motion of the wing due to translation of the body and is, therefore, a measure of the unsteadiness of the flow over the wing. Quasi-steady models become increasingly inadequate predictors of wing performance as reduced frequencies increase above 0.3 (Cloupeau *et al.* 1979; Azuma and Watanabe, 1988; Dudley and Ellington, 1990; Spedding, 1993). The observed values of the reduced frequencies in the present study (Table 1) suggest the importance of unsteady mechanisms in pectoral fin propulsion in *G. varius*.

The inferred change in the sign of the hydrodynamic attack angle (Fig. 14) and, therefore, the sign of the circulation around the fin highlights the importance of unsteady mechanisms in *G. varius* pectoral fin swimming at all speeds. A theoretical problem not addressed in quasi-steady models of lift-based locomotion is the Wagner effect, i.e. the time delay for circulation, and thus lift, to grow around an aerofoil starting from rest (Ellington, 1984; Dickinson and Götz, 1993). Until recently, the Wagner effect had only been investigated at *Re* values much greater than those relevant to the present study. Using a model wing at low *Re* (<1000), Dickinson and Götz (1993) found an unexpectedly rapid growth of lift at α_h<13.5 °. At higher attack angles, measured lift was up to 80 % *higher* after 2 chord lengths of travel than after 5 chord lengths. In the translating model, this initial pulse of high lift lasts only a few chord lengths because of eventual flow separation, causing a 'delayed' stall, but flow visualization experiments suggest that, in a translating *and flapping* wing, spanwise flow effectively prevents stall (Ellington, 1995).

The Wagner effect potentially affects forward flight only in strokes in which the direction, or sign, of the circulation differs between half-strokes, as suggested here for the bird wrasse. Dickinson and Götz (1996) have noted that, in such strokes, the vortex shed at the end of a previous half-stroke, having the same sign as the starting vortex for the new half-stroke, would increase the delay of circulation above and beyond the Wagner effect. During the downstroke in forward swimming of the bird wrasse, the hydrodynamic angle of attack changes from positive to negative *well before* the ventral phase transition, at approximately 0.67–0.78Ab. The 'additive Wagner effect' (Dickinson and Götz, 1996), if it exists, would occur during the last part of the downstroke and not during the beginning of the upstroke. At some point around the phase transition from downstroke to upstroke, the fin would shed a stopping vortex because of the change in the sign of circulation. This stopping vortex would act as the starting vortex for the upstroke (Brodsky, 1994). The resulting wake geometry should be similar to the vortex chain illustrated for the skipper *Thymelicus lineola* (Fig. 3.9 of Brodsky, 1994).

An unsteady mechanism to develop circulation rapidly around insect wings starting from rest is the 'clap-and-fling' (Weis-Fogh, 1973; Ellington, 1984). The potential vacuum created between a pair of insect wings that 'fling' open from a closed position allows the instantaneous development of circulation. Prior to the fling, the wings 'clap' together, producing a jet reaction force that may contribute to thrust (Ellington, 1984). In the bird wrasse, a pectoral fin does not fling open from its opposite fin but peels open, dorsally-to-ventrally and anteriorly-to-posteriorly, from the body. The reverse motion occurs at the end of adduction. This motion is similar to the 'squeeze-peel' described for some insects (Ellington, 1984). From our data, it is difficult to evaluate the influence of the peel-like behavior observed in the bird wrasse on the development of circulation around the fin. Daniel and Meyhöfer (1989) suggested that the squeeze mechanism should occur in fishes swimming with the pectoral fins and, indeed, Geerlink (1983) had previously observed a clap- or squeeze-like pattern in *Coris formosa* with an associated positive acceleration. In the bird wrasse, the squeeze occurs during an acceleration minimum.

When a fin speeds up or slows down, it accelerates a mass of surrounding water. The acceleration of water in one direction results in a reaction force in the opposite direction. The magnitude of the reaction force is proportional to both the magnitude of the acceleration and the mass of water accelerated (Daniel, 1984). The mean angular acceleration of an oscillating fin must be zero over a half-stroke. Nevertheless, positive linear accelerations occur in the direction of the stroke axis (Daniel, 1984), i.e. the axis within the stroke plane that lies midway between the extreme positions of the stroke. Thus, Daniel (1984) proposed that the acceleration reaction contributes to thrust in the oscillating limbs of aquatic insects and fish (this non-zero linear acceleration of an oscillating fin is also the basis for the acceleration reaction model of caudal fin propulsion in fish; Lighthill, 1975). The contribution of the acceleration reaction to thrust was explicitly excluded from early models of oscillatory fin propulsion (Blake, 1979*a*) but, following Daniel (1984), was included in later models (Morris *et al.* 1985; Blake, 1986; Gal and Blake, 1988; Williams, 1994).

In *G. varius*, the fins oscillate about a stroke axis directed dorsally, posteriorly and laterally, and the net acceleration reaction would be expected to accelerate the fish forwards and downwards (the lateral accelerations of each fin cancel). To maintain a mean height above the substratum across the stroke, *G. varius* must therefore generate upward forces to balance not only its slight negative buoyancy but also the net effect of the acceleration reaction. We can qualitatively evaluate the instantaneous influence of the acceleration reaction by comparing the acceleration of the center of mass (Fig. 5) with that of the fin (Fig. 11). During abduction, the maximum backward acceleration of the fin occurs slightly prior to the maximum forward acceleration of the center of mass and, thus, the acceleration reaction contributes to thrust during this part of the stroke. Similarly, during abduction, maximum downward accelerations of the fin occur slightly prior to maximum upward accelerations of the center of mass and, again, the acceleration reaction contributes to the net upward force on the body. During adduction, however, the center of mass has large forward accelerations between 0.2 and 0.8Ad, despite the positive forward accelerations of the fin (due to backward deceleration as it closes against the body) generating reaction forces that contribute to drag. Similarly, acceleration of the center of mass in the dorsoventral direction varies with speed during adduction despite the consistent downward accelerations of the fin. The inconsistency between fin and body acceleration suggests that acceleration reaction forces contribute only a relatively small component to the total force balance.

At the initiation of fin retraction following full abduction, the fin rays were bent by passive hydrodynamic forces so that the distal tip of the fin faced rearwards for longer than would be possible if the fin were rigid. This passive bending could potentially increase the thrust and efficiency of the oscillating fin (Katz and Weihs, 1978).

Comparisons with other flyers

The major features of pectoral fin swimming in *G. varius* present interesting comparisons with forward flight in air. On the basis of the heaving and pitching motions of the fin and the kinematics of the center of mass, we have argued for *G. varius* (1) that the fins generate thrust during both the downstroke and upstroke, with the larger contribution occurring during the upstroke, (2) that the downstroke generates an upward force, (3) that the upstroke generates an upward force at low speeds and a downward force at high speeds, and (4) that the contrasting upstroke and downstroke dynamics reflects the change in sign of the circulation between half-strokes. Similar aerodynamic conclusions have been inferred for forward flight in several insects (Weis-Fogh, 1956; Jensen, 1956; Nachtigall, 1966; Azuma and Watanabe, 1988; Dudley and Ellington, 1990; Dudley, 1991; Zanker and Götz, 1990; Wilkin and Williams, 1993) and bats (Norberg, 1976; Aldridge, 1986, 1987).

Wake visualization investigations suggest that inferred negative circulation and consequent thrust during the upstroke of bats and insects should be treated with caution. Wing strokes characterized by a change in the sign of the circulation at each half-stroke generate a vortex ‘chain’ wake, i.e. a wake presenting a pair of undulating tip vortices interconnected by transverse vortices shed during circulation transitions (Rayner, 1986; Brodsky, 1994). By contrast, a stroke in which one of the half-strokes is unloaded produces a ‘ring’ wake, while a stroke with constant circulation between half-strokes generates a ‘continuous’ vortex wake (Rayner, 1986; Spedding, 1987). Contrary to expectations based on center of mass or wing kinematics (Norberg, 1976; Aldridge, 1986, 1987), no vortex chain wakes have been observed in the steady forward flight of vertebrates, leading Rayner (1993, p. 357) to conclude that it ‘apparently does not exist in vertebrates in steady flight’.

There is similar ambiguity of the dynamic function of the upstroke in forward-flying insects. Direct force measurements indicate that the wing during the upstroke generates thrust in combination with either upward or downward forces (Cloupeau *et al*. 1979; Zanker and Götz, 1990; Wilkin and Williams, 1993; Dickinson and Götz, 1996), a pattern consistent with inferences based on wing kinematics (Jensen, 1956; Nachtigall, 1966; Azuma and Watanabe, 1988; Dudley and Ellington, 1990; Dudley, 1991). Indeed, vortex chain wakes have been observed in some forward-flying insects (Brodsky, 1994). But, in an interesting experiment, Dickinson and Götz (1996) observed a vortex ring wake, indicating the absence of aerodynamic forces on the wing during the upstroke (Rayner, 1979, 1986, 1993), coupled with direct force measurements, indicating distinct aerodynamic forces during the upstroke. Clearly, in both bat and insect flight studies, there is some inconsistency between aerodynamic inferences drawn from flow visualization and those drawn from the combination of direct force measurement, the kinematics of the center of mass and theoretical models applied to wing kinematics.

Despite these potential problems interpreting the dynamics of flapping wings or fins from kinematic data, direct force measurements and flow visualization, we predict that flow visualization studies of forward swimming in the bird wrasses or other fishes with a similar kinematic pattern will reveal a vortex chain wake, even at slow speeds. Our kinematic data support Rayner’s (1986) suggestion that negative hydrodynamic attack angles on the upstroke in aquatic flyers that are neutrally buoyant are to be expected, given that these animals need to optimize thrust and not upward forces.

Finally, we note that the kinematics of the the center of mass suggest that peak thrust is generated during the upstroke, even at the lowest speeds. This pattern contrasts with that found in vertebrate flyers in air, in which peak thrust occurs during the downstroke and the upstroke is either unloaded or generates negative thrust (but see Norberg, 1976; Aldridge, 1986, 1987). Is the generation of peak thrust during the upstroke a historical constraint or does it reflect different aerodynamic goals between vertebrates flying under water and in air? Current estimates of labrid phylogeny (Westneat, 1993; Bellwood, 1994) suggest that lift-based pectoral fin propulsion is derived, having evolved from the more primitive drag-based propulsion

several times within the Labridae. Drag-based propulsion is characterized by a distinctly loaded power stroke as the fin is rapidly adducted followed by a relatively unloaded recovery stroke during abduction (Blake, 1979*a*,*b*). This suggests that the primitive architecture of the labrid pectoral girdle made it easier to evolve a lift-based mechanism that maintained primary thrust generation during adduction and not abduction, as in birds and bats. However, kinematic data, direct force measurements and some flow visualization data suggest that the fins of *G. varius* function in a strikingly similar manner to the wings of insects. In insects, as in the bird wrasse, large upward forces are generated during the downstroke. Similarly, thrust during the upstroke is associated with downward forces at all but the lowest forward speeds. Aerial flying in insects and aquatic flying in teleost fishes are similar in two respects to aerial flying in vertebrates. First, the wings of insects and the fins of teleost fishes are thin, relatively rigid along their span and lack the multiple joints found in the forelimbs of flying vertebrates. Second, insects (in air) and fish (in water) weigh much less than birds (in air). Rayner (1986) argued that a vortex chain wake, indicating alternating signs of circulation between half-strokes, may be expected in neutrally buoyant or 'particularly light' animals, since there is less need for weight support. Bird wrasses in the size range of the individuals in this study weigh between 0.8 and 1.3 g in water, which is far less than birds and bats but approximately the same as moderate-to-large flying insects [of course, weight support is more important in a 1 g insect (in air) than in a 1 g fish (in water) because the water offers greater resistance to downward motion)]. The similarities between insect and bird wrasse kinematics and dynamics, then, suggest that the lift-based mechanism in insects and fishes has converged on a similar pattern either as a result of shared design constraints of the flapping appendage or as a common goal of thrust maximization. Clearly, it would be of general interest to explore how wake structure, or kinematic gait, scales with body size.

We thank M. Dickinson, J. Long, G. Spedding, S. Vogel, B. Wright and the University of Chicago Biomechanics Group for their suggestions and discussion regarding our ideas on fin flapping in fishes. We appreciate the reviews of the manuscript by M. Hale, B. Wright and the anonymous reviewers. This research was funded by National Science Foundation grant IBN-9407253 to M.W.W.

References

ALDRIDGE, H. D. J. N. (1986). Kinematics and aerodynamics of the greater horseshoe bat, *Rhinolophus ferrumequinum*, in horizontal flight at various speeds. *J. exp. Biol.* **126**, 479–497.

ALDRIDGE, H. D. J. N. (1987). Body accelerations during the wingbeat in six bat species: the function of the upstroke in thrust generation. *J. exp. Biol.* **130**, 275–293.

ARCHER, R. D., SAPUPPO, J. AND BETTERIDGE, D. S. (1979). Propulsion characteristics of flapping wings. *Aeronaut. J.* **83**, 355–371.

ARCHER, S. D. AND JOHNSTON, I. A. (1989). Kinematics of labriform and subcarangiform swimming in the antarctic fish *Notothenia neglecta*. *J. exp. Biol.* **143**, 195–210.

ARREOLA, V. I. AND WESTNEAT, M. W. (1996). Mechanics of propulsion by multiple fins: Kinematics of aquatic locomotion in the burrfish (*Chilomycterus schoepfi*). *Proc. R. Soc. Lond. B* **263**, 1689–1696.

AZUMA, A., AZUMA, S., WATANABE, I. AND FURUTA, T. (1985). Flight mechanics of a dragonfly. *J. exp. Biol.* **116**, 79–107.

AZUMA, A. AND WATANABE, T. (1988). Flight performance of a dragonfly. *J. exp. Biol.* **137**, 221–252.

BELLWOOD, D. R. (1994). A phylogenetic study of the parrotfishes family Scaridae (Pisces: Labroidei), with a revision of genera. *Rec. Austr. Mus.* (Suppl.) **20**, 1–86.

BLAKE, R. W. (1979*a*). The mechanics of labriform locomotion. I. Labriform locomotion in the angelfish (*Pterophyllum eimekei*): an analysis of the power stroke. *J. exp. Biol.* **82**, 255–271.

BLAKE, R. W. (1979*b*). The swimming of the mandarin fish *Synchropus picturatus* (Callionyiidae: Teleostei). *J. mar. biol. Ass. U.K.* **59**, 421–428.

BLAKE, R. W. (1980). The mechanics of labriform locomotion. II. An analysis of the recovery stroke and the overall fin-beat cycle propulsive efficiency in the angelfish. *J. exp. Biol.* **85**, 337–342.

BLAKE, R. W. (1983*a*). *Fish Locomotion*. Cambridge: Cambridge University Press.

BLAKE, R. W. (1983*b*). Median and paired fin propulsion. In *Fish Biomechanics* (ed. P. W. Webb and D. Weihs), pp. 214–247. New York: Praeger.

BLAKE, R. W. (1986). Hydrodynamics of swimming the the water boatman, *Cenocorixa bifida*. *Can. J. Zool.* **64**, 1606–1613.

BREDER, C. M., JR (1926). The locomotion of fishes. *Zoologica* **4**, 159–291.

BRODSKY, A. K. (1994). *The Evolution of Insect Flight*. New York: Oxford University Press.

CLOUPEAU, M., DEVILLERS, J. F. AND DEVEZEAUX, D. (1979). Direct measurements of instantaneous lift in desert locust; comparisons with Jensen's experiments on detached wings. *J. exp. Biol.* **80**, 1–15.

DANIEL, T. L. (1984). Unsteady aspects of aquatic locomotion. *Am. Zool.* **24**, 121–134.

DANIEL, T. L. (1988). Forward flapping flight from flexible fins. *Can. J. Zool.* **66**, 630–638.

DANIEL, T., JORDAN, C. AND GRUNBAUM, D. (1992). Hydromechanics of swimming. In *Mechanics of Animal Locomotion* (ed. R. McN. Alexander), pp. 17–49. Berlin: Springer-Verlag.

DANIEL, T. L. AND MEYHÖFER, E. (1989) Size limits in escape locomotion of carridean shrimp. *J. exp. Biol.* **143**, 245–265.

DELAURIER, J. D. (1993). An aerodynamic model for flapping-wing flight. *Aeronaut. J.* **97**, 125–130.

DICKINSON, M. H. AND GÖTZ, K. G. (1993). Unsteady aerodynamic performance of model wings at low Reynolds numbers. *J. exp. Biol.* **174**, 45–64.

DICKINSON, M. H. AND GÖTZ, K. G. (1996). The wake dynamics and flight forces of the fruit fly *Drosophila melanogaster*. *J. exp. Biol.* **199**, 2085–2104.

DRUCKER, E. G. AND JENSEN, J. S. (1996). Pectoral fin locomotion in the striped surfperch. I. Kinematic effects of swimming speed and body size. *J. exp. Biol.* **199**, 2235–2242.

DUDLEY, R. (1991). Biomechanics of flight in neotropical butterflies: aerodynamics and mechanical power requirements. *J. exp. Biol.* **159**, 335–357.

DUDLEY, R. AND ELLINGTON, C. P. (1990). Mechanics of forward flight in bumblebees. II. Quasi-steady lift and power requirements. *J. exp. Biol.* **148**, 53–88.

ELLINGTON, C. P. (1984). The aerodynamics of hovering insect flight. IV. Aerodynamic mechanisms. *Phil. Trans. R. Soc. Lond. B* **305**, 79–113.

ELLINGTON, C. P. (1995). Unsteady aerodynamics of insect flight. In *Biological Fluid Dynamics* (ed. C. P. Ellington and T. J. Pedley), pp. 109–129. Cambridge: Company of Biologists.

GAL, J. M. AND BLAKE, R. W. (1988). Biomechanics of frog swimming. I. Estimation of the propulsive force generated by *Hymenochirus boettgeri*. *J. exp. Biol.* **138**, 399–411.

GEERLINK, P. J. (1983). Pectoral fin kinematics of *Coris formosa* (Teleostei, Labridae). *Neth. J. Zool.* **33**, 515–531.

GIBB, A., JAYNE, B. C. AND LAUDER, G. V. (1994). Kinematics of pectoral fin locomotion in the bluegill sunfish *Lepomis macrochirus*. *J. exp. Biol.* **189**, 133–161.

HARRIS, J. E. (1937). The mechanical significance of the position and movements of the paired fins in the Teleostei. *Papers Tortugas Lab.* **31**, 173–189.

HILDEBRAND, F. B. (1987). *Introduction to Numerical Analysis*. New York: Dover.

JENSEN, M. (1956). Biology and physics of locust flight. III. The aerodynamics of locust flight. *Phil. Trans. R. Soc. Lond. B* **239**, 511–552.

KATZ, J. AND WEIHS, D. (1978). Hydrodynamic propulsion by large amplitude oscillation of an airfoil with chordwise flexibility. *J. Fluid Mech.* **88**, 485–497.

LANCZOS, C. (1988). *Applied Analysis*. New York: Dover.

LIGHTHILL, J. (1969). Hydromechanics of aquatic animal propulsion – a survey. *A. Rev. Fluid Mech.* **1**, 413–446.

LIGHTHILL, J. (1975). *Mathematical Biofluidynamics*. Philadelphia: Society for Industrial and Applied Mathematics.

LIGHTHILL, J. AND BLAKE, R. (1990). Biofluiddynamics of balistiform and gymnotiform locomotion. Part 1. Biological background and analysis by elongated-body theory. *J. Fluid Mech.* **212**, 183–207.

LINDSEY, C. C. (1978). Form, function and locomotory habits in fish. In *Fish Physiology*, vol. 7 (ed. W. S. Hoar and D. J. Randall), pp. 1–100. New York: Academic Press.

MORRIS, M. J., GUST, G. AND TORRES, J. J. (1985). Propulsion efficiency and cost of transport for copepods: a hydromechanical model of crustacean swimming. *Mar. Biol.* **86**, 283–295.

NACHTIGALL, W. (1966). Die Kinematik der Schlargflügelbewegungen von Dipteren. Methodische und analytische Grundlagen zur Biophysik des Insektenflugs. *Z. vergl. Physiol.* **52**, 155–211.

NORBERG, U. M. (1976). Aerodynamics, kinematics and energetics of horizontal flapping flight in the long-eared bat *Plecotus auritus*. *J. exp. Biol.* **65**, 179–212.

OSBORNE, M. F. M. (1951). Aerodynamics of flapping flight with application to insects. *J. exp. Biol.* **28**, 221–245.

PHLIPS, P. J., EAST, R. A. AND PRATT, N. H. (1981). An unsteady lifting line theory of flapping wings with application to the forward flight of birds. *J. Fluid Mech.* **112**, 97–125.

RAYNER, J. M. V. (1979). A new approach to animal flight mechanics. *J. exp. Biol.* **80**, 17–54.

RAYNER, J. M. V. (1986). Vertebrate flapping flight mechanics and aerodynamics and the evolution of flight in bats. In *Biona Report No. 5, Bat Flight – Fledermausflug* (ed. W. Nachtigall), pp. 27–74. Stuttgart: Gustav Fischer.

RAYNER, J. M. V. (1993). On aerodynamics and the energetics of vertebrate flapping flight. *Contemp. Math.* **141**, 351–400.

RAYNER, J. M. V. AND ALDRIDGE, H. D. J. N. (1985). Three-dimensional reconstruction of animal flight paths and the turning flight of microchiropteran bats. *J. exp. Biol.* **118**, 247–265.

RICE, W. R. (1989). Analyzing tables of statistical tests. *Evolution* **43**, 223–225.

SPEDDING, G. R. (1987). The wake of a kestrel (*Falco tinnunculus*) in flapping flight. *J. exp. Biol.* **127**, 59–78.

SPEDDING, G. R. (1992). The aerodynamics of flight. *Adv. comp. env. Physiol.* **11**, 51–111.

SPEDDING, G. R. (1993). On the significance of unsteady effects in the aerodynamic performance of flying animals. *Contemp. Math.* **141**, 401–419.

TRIANTAFYLLOU, G. S. (1993). Optimal thrust development in oscillating foils with application to fish propulsion. *J. Fluids Struct.* **7**, 205–224.

VIDELER, J. J. (1993). *Fish Swimming*. London: Chapman & Hall.

VOGEL, S. (1967). Flight in *Drosophila*. II. Variations in stroke parameters and wing contour. *J. exp. Biol.* **46**, 383–392.

VOGEL, S. (1994). *Life in Moving Fluids* (2nd edn). Princeton: Princeton University Press.

VOGEL, S. AND LABARBERA, M. (1978). Simple flow tanks for research and teaching. *BioSci.* **28**, 638–643.

WEBB, P. W. (1973). Kinematics of pectoral fin propulsion in *Cymatogaster aggregata*. *J. exp. Biol.* **59**, 697–710.

WEBB, P. W. (1982). Locomotor patterns in the evolution of actinopterygian fishes. *Am. Zool.* **22**, 329–342.

WEBB, P. W. (1984). Body form, locomotion and foraging in aquatic vertebrates. *Am. Zool.* **24**, 107–120.

WEBB, P. W. (1988). Simple physical principles and vertebrate aquatic locomotion. *Am. Zool.* **28**, 709–725.

WEBB, P. W. AND BLAKE, R. W. (1985). Swimming. In *Functional Vertebrate Morphology* (ed. M. Hildebrand, D. M. Bramble, K. F. Liem and D. B. Wake), pp. 110–128. Cambridge: Harvard University Press.

WEIS-FOGH, T. (1956). Biology and physics of locust flight. II. Flight performance of the desert locust (*Schistocerca gregaria*). *Phil. Trans. R. Soc. Lond. B* **239**, 459–510.

WEIS-FOGH, T. (1973). Quick estimates of flight fitness in hovering animals, including novel mechanisms for lift production. *J. exp. Biol.* **59**, 169–230.

WESTNEAT, M. W. (1993). Phylogenetic relationships of the tribe Cheilinini (Labridae: Perfciformes). *Bull. mar. Sci.* **52**, 351–394.

WILKIN, P. J. AND WILLIAMS, M. H. (1993). Comparison of the aerodynamic forces on a flying sphingid moth with those predicted by quasi-steady theory. *Physiol. Zool.* **66**, 1015–1044.

WILLIAMS, T. A. (1994). A model of rowing propulsion and the ontogeny of locomotion in *Artemia* larvae. *Biol. Bull. mar. biol. Lab., Woods Hole* **187**, 164–173.

ZANKER, J. M. AND GÖTZ, K. (1990). The wing beat of *Drosophila melanogaster*. II. Dynamics. *Phil. Trans. R. Soc. Lond. B* **327**, 19–44.